9950-639

DOE/JPL 954355/81-19
Distribution Category UC-63

Mobil Tyco Solar Energy Corporation
16 Hickory Drive
Waltham Massachusetts 02254

LARGE AREA SILICON SHEET BY EFG

Program Manager: Juris P. Kalejs

Annual Progress Report - Subcontract No. 954355

Covering Period: October 1, 1980 - September 30, 1981

Distribution Date: January 29, 1982

"The JPL Flat Plate Solar Array Project is sponsored by the U.S. Department of Energy and forms part of the Solar Photovoltaic Conversion Program to initiate a major effort toward the development of flat plate solar arrays. This work was performed for the Jet Propulsion Laboratory, California Institute of Technology by agreement between NASA and DOE."

DOE/JPL 954355/81-19
Distribution Category UC-63

Mobil Tyco Solar Energy Corporation
16 Hickory Drive
Waltham, Massachusetts 02254

LARGE AREA SILICON SHEET BY EFG

Program Manager: Juris P. Kalejs

Annual Progress Report - Subcontract No. 954355

Covering Period: October 1, 1980 - September 30, 1981

Distribution Date: January 29, 1982

"The JPL Flat Plate Solar Array Project is sponsored by the U.S. Department of Energy and forms part of the Solar Photovoltaic Conversion Program to initiate a major effort toward the development of flat plate solar arrays. This work was performed for the Jet Propulsion Laboratory, California Institute of Technology by agreement between NASA and DOE."

ABSTRACT

Progress has been made in the past year in improving ribbon flatness and reducing stress, and in raising cell performance for 10 cm wide ribbon grown in single cartridge EFG furnaces. Optimization of growth conditions has resulted in improved ribbon thickness uniformity at a thickness of 200 μm, grown at 4 cm/minute, and growth at this target speed is now routinely achieved over periods of the order of one hour or more. With the improved ribbon flatness, fabrication of large area (50 cm^2) cells is now possible, and 10-11% efficiencies have been demonstrated on ribbon grown at 3.5 to 4 cm/minute.

Factors limiting performance of the existing multiple ribbon Furnace 16 have been identified, and growth system improvements implemented to help raise throughput rates and the time percentage of simultaneous three-ribbon growth. However, this work has made it evident that major redesign of this furnace would be needed to overcome shortfalls in its ability to achieve the Technical Features Demonstration goals of 1980. This course of action did not appear to be warranted because of the age of the furnace. It was decided instead to start construction of a new multiple ribbon furnace and to incorporate the desired improvements into its design. The construction of this furnace is now completed, and it is expected to be put into operation in the last quarter of 1981.

As of October 1, 1981, the entire multiple ribbon furnace program was incorporated into the Mobil Tyco in-house program. The final status report for this portion of the program is included here.

"The JPL Flat Plate Solar Array Project is sponsored by the U.S. Department of Energy and forms part of the Solar Photovoltaic Conversion program to initiate a major effort toward the development of flat plate solar arrays. This work was performed for the Jet Propulsion Laboratory, California Institute of Technology by agreement between NASA and DOE."

TABLE OF CONTENTS

LIST OF FIGURES

LIST OF TABLES

I. INTRODUCTION

Development of EFG technology for growth of silicon ribbon has reached the point where the readiness of multiple ribbon furnaces for long term operation with acceptable duty rates and material quality must be demonstrated to establish this technology as a viable candidate for production of low-cost substrates for terrestrial solar cell fabrication. The Mobil Tyco program has worked toward this goal in the past year with the design and construction of a new multiple ribbon furnace for growth of four 10 cm wide ribbons with automatic ribbon width control and melt replenishment. At the same time, fundamental studies and optimization work continued to examine factors limiting growth performance and ribbon quality in single 10 cm cartridge furnaces.

Because of a significant change in DOE funding levels in 1981, the major part of the support for the multiple ribbon furnace program in the past year was provided by Mobil Tyco. As of October 1, 1981, the entire multiple 10 cm ribbon furnace effort has been incorporated into the Mobil Tyco in-house program. The study of factors associated with improving growth performance, and means by which to reduce stress and raise quality in 10 cm wide ribbon EFG systems is the focus of the ongoing work in the Flat-Plate Solar Array (FSA) program at Mobil Tyco still funded by DOE. This will be carried out in two single cartridge furnaces.

II. HIGH-SPEED GROWTH AND QUALITY STUDIES (J.P. Kalejs)

A. Overview

The 1981 goals for the FSA project that relate to quality and throughput for 10 cm wide ribbon growth are being addressed in two single cartridge furnaces operating under this program. Speed and quality optimization work is proceeding in Furnace 17 using a cartridge with cold shoes having growth speed capabilities of 4 cm/minute. This is aimed at development of a system for growth of uniform thickness ribbon of 200 μm (8 mils) at 4 cm/minute, which has low stress levels and can produce solar cells of 12% efficiency. The impacts on ribbon quality and stress arising from growth speed and from the cold shoe element used to increase the system speed capability are under investigation in Furnace 18 (JPL No. 1). A cartridge system which does not employ a conventional cold shoe design is being developed there for growth of 10 cm wide ribbon at speeds between 3 and 4 cm/minute.

The work associated with improving growth stability at the target speed of 4 cm/minute has proceeded on several fronts. A number of design changes in die top isotherm control elements have been made to develop isotherms that

promote ribbon edge stability and thickness uniformity. Ribbon guidance and alignment have been improved to decrease the severity of perturbations that produce ribbon deviations from flatness and growth interruptions. As a result, growth conditions have been improved to the point where uninterrupted growth at 4 cm/minute has been demonstrated over periods of one hour or more, with the limitation in growth duration often set by the charge size available in the single-cartridge furnace.

The changes implemented to improve growth conditions at 4 cm/minute and ribbon thickness uniformity have not had a noticeable impact on buckle formation, as evidenced by buckle patterns, although considerable improvement in ribbon overall flatness was demonstrable. To better understand stress generating mechanisms that may lead to buckle formation, an investigation has been started to study the relation between the ribbon post-growth temperature profile and stress-induced buckling. Significant variations in buckle patterns have been produced as a result of changes in linear cooling plate design, and in one case reduction of buckle and stress levels was achieved. These investigations are continuing to characterize the cartridge temperature fields and to develop a model to account for stresses in order that growth configurations that further reduce ribbon stress may be found.

In the course of experiments carried out in the past year designed to study the effects of various process parame-

ters on cell efficiency, it has become increasingly apparent that material property inhomogeneity occurring in high speed system grown ribbon is closely related to meniscus ambient variations. Work has accordingly focused on improving the control of ambient gas in the meniscus (growth interface) region and on studying the influence of gas species and concentrations on cell parameters. A new gas distribution system, utilizing a hollow die top shield, was introduced for this purpose. As a result of optimization studies with CO_2/O_2 in argon mixtures carried out with this system, cell efficiency has been raised to the 10-11% (AM1) range on 50 cm^2 areas for ribbon grown at 3.5 cm/minute with cold shoes. However, at its best, cell performance is still below that demonstrated on ribbon grown in the low speed (i.e., no cold shoes) systems. Experiments are now underway to examine the extent to which quality deficiency may be overcome through further optimization of growth conditions in the existing high speed growth mode. At the same time, the impact on material quality produced by growth speed and by the cold shoe itself are still of concern. Questions of the effect of specific thermal profiles on ribbon quality through stress and defect generation, the influence of speed on quality, and the possibility of cold shoe introduced impurities are all under consideration. Comparison of the material properties in growth with and without the conventional cold shoe as a function of growth parameters (speed, ribbon thickness, ambient

composition) is being planned to address these questions.

B. Experimental

1. High Speed Growth (Furnace 17)

The experiments carried out in the 10 cm cartridge with cold shoes in Furnace 17 in the past quarter are summarized in Table I. A number of changes in cartridge component design were made in a preliminary study of means by which the post-growth temperature field may be manipulated so as to influence buckle formation and ribbon stress levels. These changes included: (1) profiling the linear cooling plate to alter its cross section across the ribbon width; (2) changing of the geometry of the growth slot constriction formed by the inside surfaces of the linear cooling plates, i.e., the growth slot dimensions; (3) relocating the afterheater; and (4) increasing the length of the cooling zone of the cartridge. The most dramatic results have been achieved with the latter. The longer linear cooling plate design was originally conceived to counter seed breakage, and is described in detail in a previous report.[1] However, a significant reduction of the buckle amplitude and in residual stress levels have occurred in ribbon grown with this "stretched" cartridge. The reasons for this are not known at present. The post-growth temperature field influence on ribbon stress and buckling is the focus of ongoing work.

Table I. Run Data for 10 cm Wide Ribbon Growth in Furnace 17 in the Last Quarter. Standard Argon Flow Conditions in all Runs; 6 ℓ/minute Main Zone, 1 ℓ/minute Cartridge.

Run No.	Speed Range (cm/minute)	Comments
17-182	3.5 - 3.7	Test of profiled linear cooling plate with a hot center for purpose of studying stress generation mechanisms. Use of a single roller belt puller to study guidance perturbation effect on flatness. Buckle pattern is noticeably altered.
17-183	3.6 - 4.0	Repeat of run 17-182 but with return to old design of belt puller.
17-184	3.6 - 4.0	Repeat of 17-182. No apparent differences in flatness caused by change in puller mechanism.
17-185	2.8 - 3.0	Test of two-piece die in use in Furnace 18. Poor growth stability because of lack of bulbs at die edges.
17-186	-	Test of profiled linear cooling plates with a cold center. No growth due to poor die top temperature profile.
17-187	3.8 - 4.1	Good stability at highest speeds with hot center profiled linear cooling plates (as in run 17-182) and relocated afterheater.
17-188	3.9 - 4.0	Repeat of 17-187 with higher afterheater temperature (1130°C vs. 1095°C in 17-187). Over one hour growth without freezes at top speed. No change in buckle pattern with temperature rise observed.

Table I (Continued).

Run No.	Speed Range (cm/minute)	Comments
17-189	3.2 - 3.8	Growth of ribbon with varying thickness. No significant changes in buckle pattern with thickness observed.
17-190	-	No growth with constricted growth slot due to seed jamming and breakage.
17-191	~3	Test of additional linear cooling plate modifications. Poor growth conditions due to hot die center.
17-192	2.5 - 3.6	First test of new design "stretched" cartridge. Reasonable growth conditions. Maximum speed limited by non-optimized die top isotherms. Ribbon flatness improvement noticeable.
17-193	3.3 - 4.0	Repeat of 17-192 with hollow die shield and gas control, profiled face heater. Growth conditions good, ribbon flatness improved at highest growth speed.
17-194	3.1 - 4.0	Repeat of 17-193. Good growth conditions at 3.8 cm/minute. Ribbon flatness improved noticeably over standard cartridge-grown ribbon, stress levels lower.

2. 10 cm Ribbon System Development (Furnace 18)

Acceptable growth conditions for 10 cm wide ribbon have been established in Furnace 18 in a cartridge without cold shoes, with growth speeds up to 2.3 cm/minute. At speeds higher than this, noticeable edge instability appears because of a lack of sufficient cooling at the die ends for the given ribbon thickness. Additional cooling is to be provided by cooling tubes, or "end" cold shoes, which will cool the ribbon edges only. This system will be operated to develop a quality baseline for the 10 cm cartridge without the conventional design of cold shoe.

The experiments carried out in Furnace 18 in the past quarter are summarized in Table II. A new main zone and control electronics were installed in Furnace 18 to improve reliability of operation and to upgrade system components, respectively. Uneven main zone heating had been suspected as contributing to a lack of reproducibility of die top isotherms. Testing of the new systems occupied much of the last part of the quarter, and only a few useful growth attempts resulted. However, after the debugging period was completed, recent runs showed that better reproducibility and reliability of operation appear to have been achieved with the system improvements.

3. Material Quality Studies

A number of differences in growth conditions due to the presence of the cold shoe have been suggested as possible

Table II. Run Data for 10 cm Wide Ribbon Growth in Furnace 18 in the Last Quarter.

Run No.	Comments
18-284	Relocation of afterheater shields attempted. Poor growth conditions due to die top temperature imbalance.
18-285	Return of afterheater shields to regular location. Reasonable growth at 2 cm/minute reestablished, but edges unstable.
18-286	Test of two-piece die with saw cuts to improve edge stability. Poor growth conditions due to temperature gradients across die top.
18-287	Test of thicker profiled face heater. Poor growth conditions due to cold die center and unfavorable temperature gradient.
18-288	No growth due to broken seeds.
18-289	Initial test of end cold shoe cartridge. Water block in line prevented heatup of system. No growth attempted. Furnace and control electronics rebuilt after this run.
18-290	Cartridge without cold shoes. No growth, hot die center. Test of new control electronics and rebuilt main zone.
18-291	No growth due to afterheater shield misalignment which caused seed breakage.
18-292	No growth. Afterheater power control electronics failure.
18-293	Limited growth. Run terminated by broken seed.
18-294	Shakedown test for cartridge with end cold shoes.
18-295	Repeat of 18-293 without end cold shoes. Good growth conditions established at 2.0 to 2.3 cm/minute. Ribbon edge instabilities appear at 2.5 cm/minute.

causes for quality deficiency of ribbon grown in this high speed mode.[2] This deficiency has been manifested as a generally lower cell efficiency of 10 to 11% (AM1) for material grown with the cold shoes, than the 11+% level demonstrated in growth at 2 cm/minute without cold shoes.[3] Correspondingly, as-grown material SPV diffusion lengths for the former more often have fallen into the range of 30 to 40 μm, rather than the levels of 40 to 50 μm achieved without cold shoes. Material inhomogeneity, as evidenced by diffusion length variations across the width of 10 cm ribbon, has been more severe and more sensitive to ambient conditions for the ribbon grown with cold shoes than without, accounting for much of this difference. The best small area (1 cm^2 diameter) SPV barriers within a ribbon width span often have been as high as 50 to 70 μm. SPV L_D fluctuations appear to be related to the manner that gas is introduced into the interface region, viz., location of gas sources, gas flow patterns and velocities, as well as to gas species and composition. A new gas distribution system was developed in the past year to improve control of interface ambient gases. This has had an impact in generally raising the reproducibility and consistency of experimental data, and helping to achieve 10-11% cell efficiency over larger (50 cm^2) areas (see Section IV for details). However, better control of interface gas conditions is still needed. In particular, the main zone purge gases exit through the interface region and growth slot, and

this imposes a major uncertainty as to the steady-state gas flow pattern and individual gas species concentration levels near the interface. Design efforts are underway to reintroduce an improved gas seal at the ribbon exit and allow the main zone gases to be re-routed (see also Section III). This will be done in the next quarter.

Considerable experimental data has been gathered regarding the dependence of ribbon and cell parameters on such process variables as ambient gas flow conditions, species (CO_2, CO and O_2) and concentration, quartz in the melt as a source of oxygen, resistivity and growth speed. The ambient gas species concentration of CO_2 and O_2 emerges as the most important influence on cell efficiency at a given doping level. For the given gas distribution system, CO_2/O_2 in argon mixtures with CO_2/O_2 levels in the range from (2000 to 5000 ppm)/(20 to 50 ppm) have been shown to be required to optimize cell performance at the 10-11% level. These are the gas concentrations introduced into the cartridge. The interface gas concentrations are not known, but estimates made on the basis of ribbon surface film cover produced by a given level of CO made in earlier runs[4] would suggest a range of 100 to 300 ppm of CO was present in the environment of the growing ribbon. At this point, no specific difference between CO_2 or CO in influencing cell properties has been identified. CO_2, to which a low level of O_2 has been added, has been used for most of the work, however. These gases

have been chosen because of a generally lower incidence of SiC, both in die top deposits and ribbon film, arising from this higher oxygen level, and because of the evidence that ribbon interstitial oxygen levels are higher at a given gas concentration level. Thus, lower concentration levels can be used. No correlation of cell efficiency with interstitial oxygen level is evident on the basis of the data obtained to date.

4. Future Work

The two major problems that will be addressed in future work relate to understanding of mechanisms that induce stress in ribbon during growth and to identifying factors that control ribbon quality in the cold shoe system. Fundamental studies that examine basic phenomena in these areas are planned. The program on study of ribbon stresses will: (1) characterize cartridge temperature fields as a function of linear cooling plate design; (2) initiate modeling of temperature-stress relationships that can identify mechanisms of stress generation and ribbon buckling. Work on quality improvement will proceed both through implementation of changes in the growth area, and with the study of processes by which ribbon properties are influenced in high temperature annealing. In the growth area, an improved cartridge ambient control system and gas distribution means will be sought, and ribbon will be grown with and without the conventional cold shoe design to obtain a quality comparison. Another aspect

of this work will be to test the effect of different designs and materials of construction for cold shoes and power leads (containing the only metals in the cartridge) on ribbon quality. These growth parameter investigations will be supplemented by basic studies on the effect of high temperature heat treatments on ribbon properties (see also Section IV).

III. MULTIPLE RIBBON GROWTH SYSTEM DEVELOPMENT (B.H. Mackintosh)

A. Overview

The multiple ribbon furnace program has undergone a number of changes in direction in the course of the past year. Operation of the original multiple ribbon Furnace 16, rebuilt in 1980 to accommodate three cartridges for 10 cm wide ribbon, has gradually been de-emphasized because of increasing reliability problems. All operation of this furnace ceased in July 1981 after a number of multiple growth runs in the last quarter of 1980 and first quarter of 1981. These revealed shortcomings of this machine in both throughput and product quality, which require that problems in a number of areas be addressed before acceptable performance levels can be expected.[3] With these in mind, the design and construction of a new multiple ribbon furnace for growth of four 10 cm wide ribbons was started in the first quarter of 1981. This furnace was to be built at Mobil Tyco's expense and to be incorporated into the JPL program for operation in the last quarter of 1981. Construction of the furnace has proceeded on schedule, and the furnace is to be put into operation in the last quarter of 1981 as planned. However,

the JPL program at Mobil Tyco has been reduced in scope and will concentrate on research on fundamental problems of stress reduction in ribbon and on quality improvement in high speed growth in single cartridge furnaces. All multiple ribbon furnace development within the program will cease as of October 1, 1981. The description of the concepts that are part of the multiple ribbon furnace updated design, therefore, are presented in what follows as a final status report for this portion of the JPL program.

B. Multiple Ribbon Furnace Development

The design and construction of a new multiple ribbon furnace was undertaken in early 1981 when it became evident that Furnace 16 would not be capable of fulfilling the Technical Features Demonstration goals set for it in 1980 without a major redesign effort. These goals called for a multiple ribbon growth run of eight hours, a growth rate of 4.5 cm/minute, a machine duty rate of 85% or better, operational automatic controls on one ribbon, and a ribbon quality sufficient for 10.2% cell efficiency. The shortfall in meeting these goals was shown to be caused partly by cartridge-related deficiencies, and partly by main zone furnace inadequacies.[3] The program plan for 1981 accordingly called for optimization work on the cartridge with respect to growth performance and ribbon quality to continue in single cartridge furnaces during the construction phase of the new furnace. Prior to proceeding with this course of action, a

standardization of cartridge components, and main zone configuration insofar as was possible, was carried out to place cartridge performance in both multiple and single cartridge furnaces on a comparable level. The elements of design that are to be incorporated into development of the new multiple ribbon furnace are examined in more detail next. Main furnace and cartridge-related topics are discussed under separate headings.

1. Main Zone Furnace Design

The new multiple furnace will allow for growth of four 10 cm wide ribbons, as compared to three for the present Furnace 16. This provides a more symmetric configuration for locating two cartridges on either side of a central melt replenishment unit. The new furnace is shown in the photograph in Figure 1. The target operating growth speed has been lowered to 4 cm/minute from the previous 4.5 cm/minute, and the extra cartridge provides more than the necessary compensation for the decreased areal throughput resulting from this speed reduction. The lower growth speed has been shown to be attainable with the existing cooling capabilities in the cartridge already in use, and limits the experimentation necessary to improve performance to acceptable levels only to optimization studies.

A new melt replenishment unit is to be incorporated into the updated furnace design. The original design had proved to be unreliable when pushed to the limit even for supplying

Figure 1. Multiple ribbon furnace for growth of four 10 cm wide ribbons.

silicon for growth of three 10 cm wide ribbons. The new unit will have the capability to provide for growth of four ribbons, and will utilize silicon chips rather than the specially shaped solid charge rod used in the old unit.

Additional changes that have been incorporated into the new furnace design will improve main zone insulation, the furnace jacket cooling arrangement, and power supplies to provide for more efficient operation of the main zone.

2. Cartridge Performance

The outstanding factor contributing to the productivity shortfall in multiple ribbon growth demonstration runs was related to seed ribbon breakage. This breakage occurred frequently enough to cause appreciable loss of growth time and cartridge performance degradation due to broken silicon seed pieces melting on the die and becoming jammed in the growth slot. The cause of this was recognized as stress increases in seeds being inserted into the upper regions of the cartridge growth slot caused by an abrupt decrease in temperature at the cartridge exit. A new elongated or "stretched" cartridge has been designed to change the temperature profile at the linear cooling plate termination, as illustrated in Figure 2. This design has undergone preliminary testing in Furnace 17 (see Section II). A detailed description of this cartridge appears in an earlier report.[1]

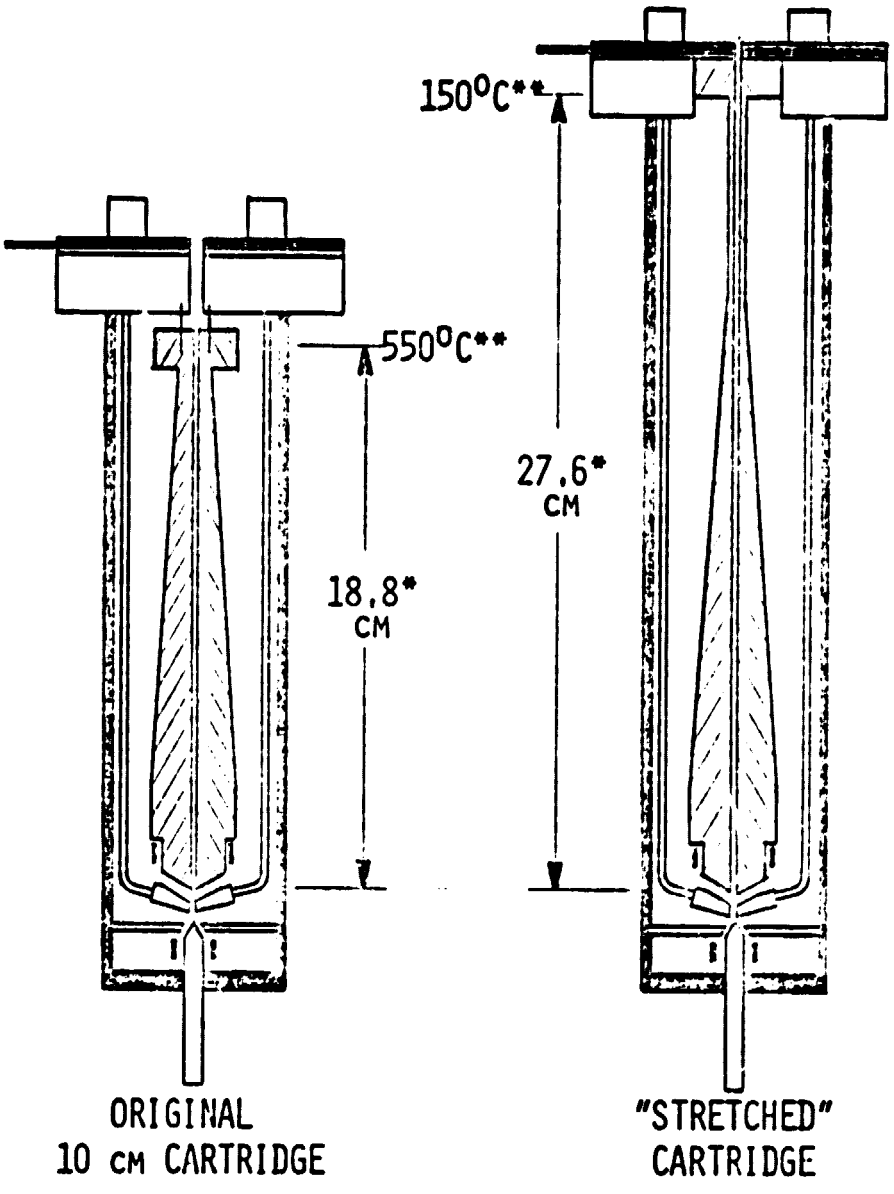

*EFFECTIVE LENGTH OF LINEAR COOLING PLATES.

**ENDING TEMPERATURE OF CONTROLLED GRADIENT REGION.

Figure 2. New cartridge (on right) designed to alleviate seed breakage problem.

Aspects of cartridge design that impact on ribbon quality have been under study in the single cartridge furnaces. Ambient gas flow pattern and composition control has been demonstrated there to have a first order effect on ribbon cell performance.[1] The gas distribution system in use has not been developed specifically for use in a multiple furnace environment, where implementation of any control poses special problems because of the multiplicity of openings (at the cartridge locations and the melt replenisher). A means to seal off the ribbon exit at each cartridge location is under development at present. This is illustrated in Figures 3 and 4. In the present arrangement, all the main zone gases are flushed through the cartridge growth slot (Figure 3). Although this arrangement does not impede successful implementation of a gas control system in the single cartridge furnace, this is not the case for the multiple ribbon furnace because the main zone purge gas flow is distributed among several cartridge openings. Different flow resistances generally exist at each of the cartridge locations, and thus a constant flow rate at any one location cannot be guaranteed. In the gas control system under development, complete control of the cartridge ambient will be sought by sealing each ribbon exit, as illustrated in Figure 4.

A number of other refinements of control electronics are due to be implemented to improve overall furnace operation and reliability. These include automatic width control

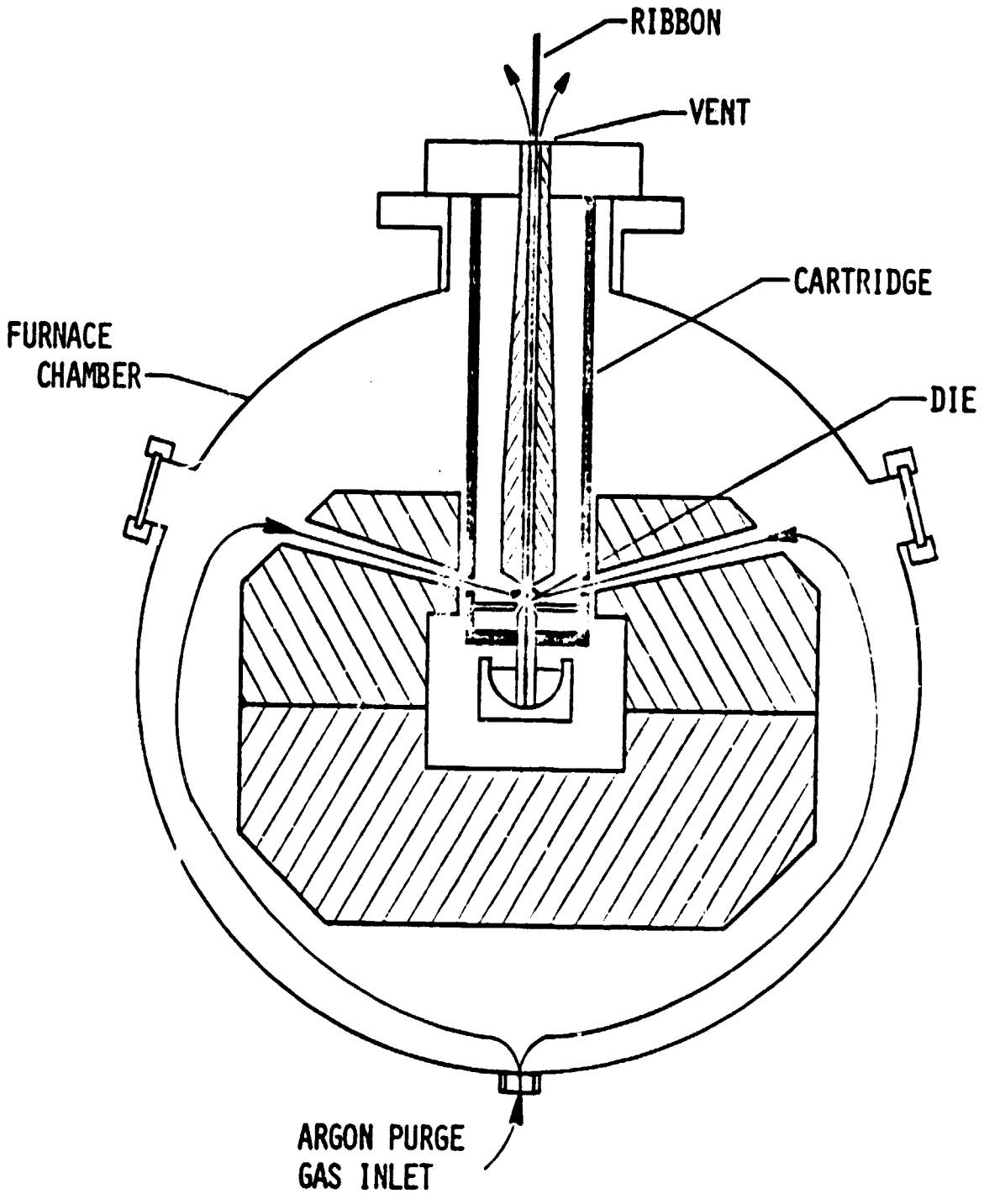

EFG FURNACE WITHOUT RIBBON SEAL

A LARGE PURGE GAS FLOW PREVENTS BACKSTREAMING, BUT ENTRAINS ALL GAS SPECIES PRESENT IN THE FURNACE PAST MENISCUS AND HOT RIBBON.

Figure 3.

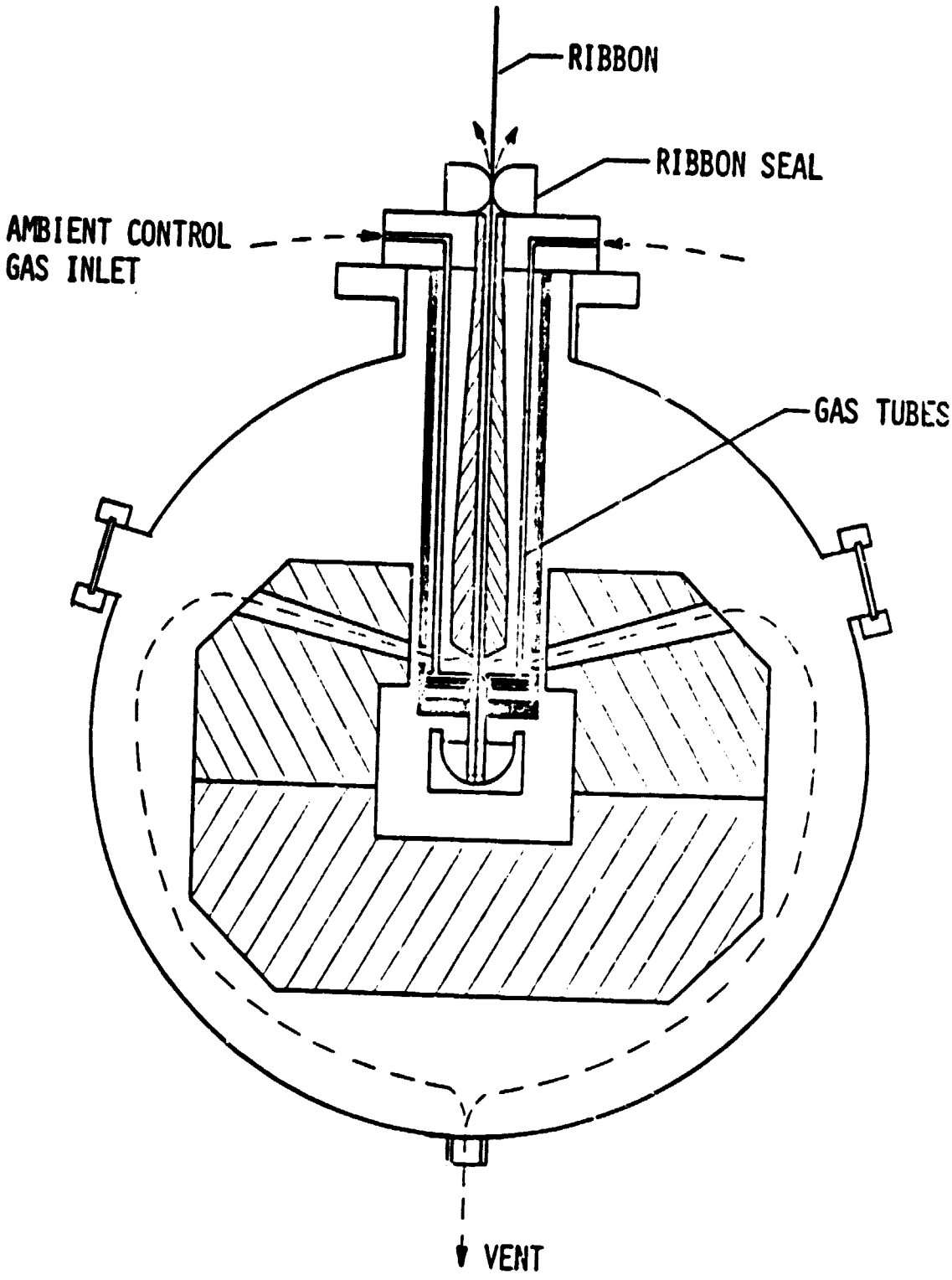

EFG FURNACE WITH RIBBON SEAL

PURGING GAS OF CONTROLLED COMPOSITION IS ADDED THROUGH THE CARTRIDGE AND DIRECTED AT THE GROWTH INTERFACE

Figure 4.

system improvements tested during the past year, and improved cartridge power supplies. Finally, the new multiple furnace is to be housed in a specially constructed room with humidity control, filtered air, and non-particulating surfaces to reduce the possibility of contamination from the general furnace environment.

IV. CELL AND MATERIAL CHARACTERIZATION (L.A. Ladd)

A. Overview

During 1980, growth parameters were developed for Machine 18 which resulted in the ability to consistently grow ribbon with diffusion lengths of 40 to 50 μm and which could be made into solar cells with 11-12% average efficiency. These conditions involved the growth of 5 cm wide ribbon at 2 cm/minute and incorporated the injection of a gas containing CO_2 from above the interface. Our objectives for 1981 were to learn how to reproduce this result with 10 cm wide ribbon grown in a system with cold shoes. Preliminary results obtained in 1980 indicated a new gas distribution system configuration would yield ribbon with diffusion lengths between 30 and 40 μm and cells with 9-10% efficiency. The CO_2 concentration and resistivity levels were optimized in the course of this year and it was determined that average run efficiencies of 10-11% could be achieved for large area cells. It is believed, however, that more fundamental changes will be required to get average efficiencies of above 11%.

In Section B, the work which was done to optimize the CO_2 concentration and resistivity will be summarized. The data which have been presented in previous reports will for the most part not be included again in this report. Section B will also include work which was done to evaluate the use of quartz in the melt as an alternative method of introducing oxygen into the ribbon. In Section C, heat treatment experiments which have been started will be discussed. The purpose of these experiments is to determine how ribbon grown under various conditions responds to high temperature heat treatment. This information will be used to gain a better understanding of what the limiting material factors are that govern ribbon diffusion length and will, it is hoped, lead to an understanding of what fundamental changes are required in order to grow ribbon suitable for making high efficiency cells.

B. Cell Characterization

The main effort in this area this year has been to optimize quality and growth parameters for 10 cm wide ribbons grown at greater than or equal to 3.5 cm/minute in Machine 17. Various gas ambient conditions in the growth cartridge have been evaluated. For the most part a gas mixture of 1% CO_2 plus 100 ppm O_2 in argon, which is then diluted further in argon, has been used in the cartridge. Some of the work earlier in the year was done using a 1% CO_2 in argon gas mixture which was then diluted further in argon. The results

were similar. The conclusion of this work is that the best ribbon diffusion lengths and the best cell performance for phosphine processed cells take place for concentrations of between 0.1% CO_2 plus 10 ppm O_2 and 0.5% CO_2 plus 50 ppm O_2. For these ambient gas conditions, ribbon diffusion lengths of from 30 to 40 μm can be consistently obtained and average cell efficiencies of between 10% and 11% efficient cells can be achieved. This applies to both large and small area cells.

Table III shows data obtained earlier this year for large area (50 cm^2) cells from run 17-143. A total of nine cells were processed and tested and two had high reverse leakage current and are not included in the table. The average efficiency is 9.6%. This ribbon was grown at 2.5 cm/minute with between 0.2% CO_2 and 0.33% CO_2 applied to the growth cartridge. Table III also shows data obtained from a batch of large area cells processed from a number of recently grown runs. The ribbon for all of these recent runs was grown at 3.5 cm/minute. For the two runs which were grown under near optimum conditions, the average cell efficiency is 10% or greater. For the current growth setup, higher efficiency cells were achieved at a higher growth speed. This demonstrates that for the current growth setup the speed is not a first order parameter in affecting cell performance.

Table IV summarizes the results obtained for phosphine processed small area (6 cm^2) cells for various gas ambient

Table III. Solar Cell Data for Phosphine Processed Large Area (50 cm^2) Solar Cells Made from 10 cm Wide Ribbons.

100 mW/cm^2, Xenon Light, 28°C, AR Coated.

Run No.	Growth Ambient	Speed (cm/min)	Average Resistivity (Ω-cm)	Diffusion Length (μm)	Cell Parameters				
					J_{sc} (mA/cm^2)	V_{oc} (V)	FF	η (%)	Mean η (%)
17-143	0.2% CO_2	2.5	1.5	27	26.5	0.523	0.608	8.4	9.6
					26.5	0.531	0.705	9.9	
					27.7	0.534	0.677	10.0	
					26.2	0.530	0.699	9.7	
					28.6	0.538	0.634	9.7	
					26.2	0.529	0.717	9.9	
					26.6	0.533	0.896	9.9	
17-174	Quartz in melt	3.5	1.0	35	25.3	0.527	0.667	8.9	9.4
					26.7	0.534	0.697	9.9	
17-175	0.3% CO_2 + 30 ppm O_2	3.5	1.0	36	26.8	0.539	0.735	10.6	10.3
					27.7	0.545	0.706	10.7	
					26.1	0.537	0.720	10.1	
					27.5	0.547	0.641	9.7	
17-178	1% CO_2 + 100 ppm O_2	3.5	1.0	34	26.4	0.518	0.696	9.5	9.1
					26.2	0.517	0.642	8.7	
17-181	0.23% CO_2 + 23 ppm O_2	3.5	4.0	43	29.0	0.525	0.603	9.2	10.0
					28.8	0.522	0.713	10.7	

Table IV. Summary of Averaged Solar Cell Data for 10 cm Wide Ribbon Grown with Varying Melt Doping Levels.

ELH Light, 100 mW/cm^2, $28^{\circ}C$, No AR Coating.

Run No.	Melt Doping (Ω-cm)	Measured ρ (Ω-cm)	Speed (cm/min)	Growth Ambient (% CO_2/ppm O_2)	Cell Parameters				CZ
					J_{sc} (mA/cm^2)	V_{oc} (V)	FF	η (%)	η (%)
17-177-1A	0.2	0.3	3.5	0 / 0	11.7	0.510	0.753	4.5	10.0
17-179-1B		0.3	3.5	0.5 / 50	14.7	0.540	0.745	5.9	10.0
17-117	1.0	1.2	3.8	0 / 0	13.7	0.486	0.747	5.0	10.9
17-162-1A		1.1	3.2	0 / 0	15.6	0.503	0.762	6.0	10.7
17-175-1C		1.2	3.5	0.3 / 30	17.3	0.534	0.732	6.8	9.8
17-178-1B		1.6	3.5	0.5 / 50	16.8	0.524	0.750	6.6	9.8
17-178-1E		1.6	3.5	1.0 /100	16.0	0.518	0.723	6.0	9.8
17-139-1B	4.0	5.4	3.2	0 / 0	15.5	0.470	0.734	5.4	9.8
17-136-2A		5.9	3.1	0 / 0	15.8	0.472	0.681	5.1	10.0
17-136-2B		6.0	3.0	0.14/ 14	18.6	0.519	0.717	6.9	10.0
17-181-1B		3.5	3.5	0.23/ 23	18.2	0.512	0.736	6.9	10.0
17-139-2A		5.0	3.3	0.23/ 0	19.0	0.513	0.753	7.3	9.8
17-136-2C		5.9	3.1	0.33/ 33	19.2	0.524	0.746	7.5	10.0
17-181-1D		3.5	3.5	1.0 /100	17.4	0.512	0.745	6.6	10.0

conditions and various ribbon doping levels. As can be seen from the table, the optimum doping level is from 1-4 Ω-cm and the optimum CO_2 concentration is between 0.1% and 0.5%. The column on the right-hand side of the table indicates the cell efficiency that was obtained for CZ control samples that were processed along with the ribbon samples. This gives an indication of the process variability and allows spurious data to be rejected. The efficiencies of the two runs which had unusually high efficiency CZ cells should probably be scaled down somewhat. Since the efficiency of cells typically increases by 45% when the cells are AR coated, this means that a 6.9% non-AR coated cell will become a 10% cell after AR coating. The data in the table thus clearly confirm the result that by using optimized CO_2 ambients average cell efficiencies in excess of 10% can be achieved in Machine 17.

The CO_2 effect has also been demonstrated in Machine 16 and average efficiencies of about 9% have been achieved. This is acceptable considering that very little optimization work was done there because of non-standard operating procedures.

The use of a gas containing CO_2 plus O_2 in the growth cartridge produces two measurable effects: (1) raises the interstitial oxygen level of the ribbon, and (2) produces a film on the ribbon. The level of interstitial oxygen has been measured by infrared spectroscopy on a number of samples. A correlation between interstitial oxygen levels and

CO_2 concentrations has not been found and there is a lot of scatter in the data. It has also been found that as the CO_2 concentration is increased, the interstitial oxygen first increases and then decreases. The highest values of interstitial oxygen correspond roughly to the level of CO_2 for which the best cell performance is obtained. This dependence of interstitial oxygen level on CO_2 concentration indicates that there are several reactions taking place. Apparently, some of the processes increase the flux of oxygen into the meniscus while others impede it. It may also be that the film on the ribbon (during the ribbon transit of the afterheater region) affects ribbon properties. A series of experiments to understand better what happens when ribbon is heat treated has been initiated and is discussed in the next section.

Adding quartz to the melt as an alternative method of introducing oxygen into the ribbon has also been investigated. The results have, however, not been nearly as consistent as the results with using a CO_2 (plus O_2) gas mixture in the growth cartridge. Large variation in the amount of oxygen introduced into the ribbon and in the solar cell performance has been observed, and no significant trends have been identified.

C. Heat Treatment Experiments

One major problem in making high efficiency cells has been that carbon crucible-grown ribbon has typically had

lower diffusion lengths and short circuit currents than quartz crucible-grown ribbon when PH_3 processed. Previous experiments indicate that the ribbon diffusion length is sensitive to heat treatment and may be degraded by the phosphine diffusion process. It has also been shown that the introduction of a small amount of CO_2 gas into the growth cartridge can improve both ribbon diffusion length and cell performance and that this usually results in a higher level of interstitial oxygen in the ribbon. Thus, a series of experiments has been started in order to determine in more detail the effects of heat treatment of ribbon properties, and, if possible, to determine what the role of oxygen is in influencing ribbon diffusion lengths and cell performance. The objective of these studies will be to learn how to grow ribbon with higher diffusion lengths and how to process the ribbon so as to preserve or even improve the diffusion length in order that the program cell efficiency goals can be met.

This is quite a broad area to investigate, and to begin with, some basic annealing studies have been performed to determine the effect of various heat treatments on ribbon properties. In interpreting these results, both bulk and surface effects have to be taken into account. The bulk effects have to do with the diffusion, interaction, and clustering or precipitation of impurities, oxygen, carbon, and defects. The surface effects have to do with the fact that, depending on the ambient, interstitials, vacancies and

other types of defects can be generated or annihilated at the surface of the ribbon during heat treatment. Some of these defects have very high diffusion coefficients and can move throughout the bulk of the sample during heat treatment and effect changes in the bulk material properties. For certain types of anneal parameters (e.g., oxidation), gettering of impurities can also take place at the sample surface. Thus, the annealing results may depend on the time and temperature of the anneal and the ambient in which the anneal is performed. The results will also depend on the following properties of the as-grown ribbon: doping level, impurity type and level, defect type and density, and oxygen and carbon levels. A more extensive theoretical discussion and review of the literature will be included in a later report.

The initial experiments were made using sample pairs obtained by cutting two one-inch square pieces positioned adjacent to one another along the growth direction. One sample was used for the anneal and one sample was used as a control or "sister" sample. After the heat treatment, aluminum contacts were formed on the back of both samples by evaporation followed by sintering at 575^{o}C, and a front aluminum layer was then evaporated to make a Schottky barrier. The diffusion lengths of both the annealed samples and the sister samples were then measured using the standard SPV apparatus.

Initial results have shown that the nonuniformity of the ribbon introduces considerable scatter in the data and trends may be difficult to identify. The preliminary conclusions which can be drawn from the experiments which have been done are as follows: (1) Heat treatment in nitrogen and oxygen at 1000°C for one hour causes a severe degradation in diffusion length of from 30% to 80%. (2) The magnitude of the degradation does not seem to depend on the ribbon doping level in the range from 1 Ω-cm to 30 Ω-cm, on the interstitial oxygen level in the ribbon, or on whether the anneal is done in oxygen or nitrogen.

Further work which is planned in this area will involve two main sets of experiments: (1) experiments to determine the effect of time, temperature and ambient conditions on ribbon annealed at intermediate temperatures such as might be used in cell processing (700°C to 1100°C). In addition to the effects of oxygen, nitrogen and argon ambients, the effects of different diffusion conditions will also be investigated; and (2) experiments to determine the effect of time, temperature and ambient conditions on ribbon annealed at high temperatures such as the ribbon undergoes during the afterheat cycle immediately after solidification in the growth cartridge (1100°C to 1300°C). In both these regions the effect of the anneal on the minority carrier diffusion length and on the light enhancement effect will be studied for ribbon grown with and without cold shoes and with differ-

ent growth ambient conditions. These experiments should lead to a better understanding of the basic materials parameters that govern ribbon diffusion length and should enable the growth parameters to be optimized for growing ribbon that can be made into high efficiency cells. The main emphasis is on improving ribbon diffusion length, since this is the chief shortcoming of the material that is currently being grown.

REFERENCES

1. J.P. Kalejs et al., "Large Area Silicon Sheet by EFG," Second Quarterly Report, DOE/JPL 954355/81-18 (Covering Period: April 1, 1981 - June 30, 1981).

2. F.V. Wald et al., "Large Area Silicon Sheet by EFG," Annual Progress Report, DOE/JPL 954355/80-3 (Covering Period: October 1, 1979 - September 30, 1980).

3. J.P. Kalejs et al., "Large Area Silicon Sheet by EFG," First Quarterly Report, DOE/JPL 954355/81-17 (Covering Period: January 1, 1981 - March 31, 1981).

4. F.V. Wald et al., "Large Area Silicon Sheet by EFG," Fourth Quarterly Report, DOE/JPL 954355/79-4 (Covering Period: October 1, 1979 - December 31, 1979).

APPENDICES

1. Updated Program Plan

An updated program plan went into effect on March 1, 1981.

2. Man Hours and Costs

Previous cumulative man hours were 100,661 and cost plus fixed fee was $3,657,319. Man hours for October 1980 through September 1981 are 19,547 and cost plus fixed fee is $792,435. Therefore, total cumulative man hours and cost plus fixed fee through September 1981 are 120,208 and $4,449,754, respectively.

3. Engineering Drawings and Sketches Generated During the Reporting Period

None.

4. Summary of Characterization Data Generated During the Reporting Period

See Section IV.

5. Action Items Required by JPL

None.

6. New Technology

Any new items of technology will be separately reported pending possible patent action.

7. Other

As-grown material supplied to JPL.

8. Publications

(a) "Modeling of Ambient-Meniscus Melt Interactions Associated with Carbon and Oxygen Transport in EFG of Silicon Ribbon," by J.P. Kalejs and L.-Y. Chin, accepted for publication in Journal of The Electrochemical Society. (b) "Some Aspects of the Effect of Heat Treatment on the Minority Carrier Diffusion Length in Low Resistivity p-Type Silicon," by C.T. Ho and F.V. Wald, phys. stat. sol.(a) 67, 103 (1981).

APPENDIX 7

AS-GROWN MATERIAL SUPPLIED TO JPL

Ribbon 17-130

Grown on Machine 17
Purified graphite cartridge and furnace components
Melt doped to 1 Ω-cm
Sample size 5 cm x 10 cm (2" x 4")
Speed 3.2 to 3.6 cm/minute

Ribbon 17-132

Grown on Machine 17
Purified graphite cartridge and furnace components
Melt doped to 1 Ω-cm
Sample size 5 cm x 10 cm (2" x 4")
Speed 2.8 to 3.4 cm/minute

Ribbon 17-176

Grown on Machine 17
Purified graphite cartridge and furnace components
Melt doped to 1 Ω-cm
Sample size 5 cm x 10 cm (2" x 4")
Segment 1B slow, thick (2.5 cm/minute)
Segment 2C fast, thin (3.8 cm/minute)

APPENDIX 8(a)

MODELING OF AMBIENT-MENISCUS MELT INTERACTIONS ASSOCIATED WITH CARBON AND OXYGEN TRANSPORT IN EFG OF SILICON RIBBON

J.P. Kalejs

Mobil Tyco Solar Energy Corporation

16 Hickory Drive

Waltham, Massachusetts 02254

L.-Y. Chin[1]

Department of Chemical Engineering

Clarkson College of Technology

Potsdam, New York 13676

ABSTRACT

Impurity transport processes associated with interaction of reactive ambient gases and meniscus melt during growth of silicon ribbon by the Edge-defined Film-fed Growth (EFG) technique have been investigated with the help of numerical solution of mass and momentum transport equations. The transport of oxygen and carbon is examined in detail. It is shown that oxygen transport from meniscus sources can account for the interstitial oxygen observed to be introduced into ribbon grown with CO_2 in the meniscus ambient. Growth speed is the process parameter which has the most pronounced influence on ribbon impurity levels when a source or sink for the impurity is present on the meniscus surface.

[1]Present address: Phillips Petroleum Co., Bartlesville, Oklahoma 74004.

Key words: Mass transport, growth model, impurity, EFG silicon ribbon.

Ambient gases CO and CO_2 have been used to influence the properties of silicon ribbon produced by the Edge-defined Film-fed Growth (EFG) technique (1). Changes in the structure and improvements in the electronic properties of the ribbon for the purpose of making solar cells have been demonstrated. The processes that are responsible for these effects lead to changes in ribbon carbon and oxygen levels. The purpose of this paper is to examine the manner in which these processes affect impurity transport in the growth interface melt using numerical solutions of the mass and momentum transport equations.

Ambient gas composition variations have been used to produce carbon and oxygen concentration changes in silicon crystals grown by the float zone (2) and Czochralski (3) methods. The experiments with silicon ribbon grown by the EFG technique differ from these earlier studies in several respects. The growth system under consideration is shown in schematic in Figure 1. New features of this system are the graphite crucible used to contain the bulk melt, and the die, also made of graphite. The latter contains the capillary path which connects the crucible to the die top and to the meniscus, or growth interface region. The die acts to isolate the interface melt from that in the crucible. This isolation allows die top melt transport processes to be considered independently of those operative in the crucible. Crucible conditions are important only insofar as they fix

average impurity levels of the melt entering the die capillary. Except for carbon, these levels are expected to remain unchanged during the melt traverse of the capillaries because they are located internally to the die. Carbon melt transport involves special considerations due to the continued reaction of silicon melt and the graphite die taking place during crystallization flow from the crucible to the interface.

Since a graphite crucible is used to contain the bulk melt, oxygen and SiO gas are not produced by interaction of the melt and the crucible material, such as occurs with the use of silica crucibles in conventional Czochralski growth. Sources of oxygen other than the crucible may exist, e.g., residual oxygen in the charge material and furnace gases in the bulk melt ambient. For the purposes of the present study, the only processes considered to alter the carbon and oxygen concentrations in the melt after it has entered the die are those associated with reactive gas species at the meniscus surface. These gases are introduced to the interface region via the gas tubes shown in Figure 1.

Carbon and Oxygen Sources in Ribbon Growth

Ambient gas-meniscus reactions shown to influence ribbon properties have involved the gases CO and CO_2. They have been introduced into the growth system at partial pressures that typically range from 1×10^{-3} to 1×10^{-2} atm in a carrier gas of argon. Interface melt ambient partial pressures

of reactive gases are estimated to be in the range from 1 x 10^{-5} to 1 x 10^{-3} atm (1), and the gases are predominantly CO and SiO. Ribbon growth speeds varied from 0.03 to 0.05 cm/s in these experiments, with thicknesses of 200 to 300 μm.

Thermodynamic considerations for typical growth system temperatures (1685^{o}K) and reacting gas partial pressures (~10^{-3} atm) show (4) that reactions of CO with silicon melt can produce SiC, SiO_2 and SiO. The latter two compounds are known to act as sources of oxygen for silicon melt. These same oxygen sources are generated when CO_2 is used. The conditions under which CO_2 is introduced, temperatures above 1000^{o}C and in the presence of carbon parts, favor conversion of the CO_2 to CO. At the same time, the partial pressure of oxygen will be higher with CO_2 than CO and will impact on the balance of reaction products. Kaiser et al. (2) have examined relationships between the oxygen content of silicon crystals solidified in the presence of ambient oxygen and its partial pressures and flow rates. They find that the oxygen reaches its saturation value in silicon at a gas partial pressure of about 8 mm of Hg (~1 x 10^{-2} atm). At higher pressures, no further reaction occurs because the melt surface is passivated by the formation of a film of SiO_2. The maximum interstitial oxygen concentration observed is 2 x 10^{18} at/cc, or 69 ppma, based on the ASTM procedure F-121. This value is taken as a limit to the oxygen concentration available at a melt surface to act as a source for the diffu-

sion phenomena that are modeled in the present calculations.

The reactions of CO and CO_2 with silicon melt, considered as sources for oxygen, also affect dissolved carbon levels (3). In EFG with graphite crucibles and dies, the meniscus melt already has high levels of carbon. Additional carbon will not go into solution if the melt is saturated. The formation of SiC is then a likely process by which the carbon brought to the meniscus surface by the gas can be accommodated. Growth of SiC particles will proceed in regions of the meniscus where carbon supersaturation occurs (1). Meniscus surface film, presumed to be a mixture of SiC and SiO_2, is observed at high CO and CO_2 ambient concentrations when no growth is taking place. Under dynamic growth conditions the surface film is continuously incorporated into the growing ribbon, which frees the meniscus surface for additional SiC nucleation and growth. This provides a sink for meniscus carbon that is operative under steady-state growth conditions.

It is also possible to achieve experimental conditions for which removal of carbon and oxygen from the meniscus surface takes place by evaporation. For example, oxygen may be depleted from the melt either as SiO or together with carbon as CO (5), provided sufficiently low partial pressures of these gases exist at the melt surface (here, the meniscus).

The aim in the present calculations is to predict the response of melt carbon and oxygen distributions to changes

in ribbon growth conditions given that ambient gases and their reaction products act as sources or sinks for these impurities at the meniscus surface. Average impurity concentrations and distributions through the ribbon thickness are obtained as a function of ribbon thickness, growth speed and meniscus height.

Impurity Transport Calculations

Numerical methods for calculation of impurity transport and redistribution in the interface melt region for ribbon EFG are discussed in detail elsewhere (6,7). The present results have been obtained with the help of the solutions of the heat and momentum transport equations of Reference 7. Interface shapes and velocity fields were obtained there for a domain encompassing a plane through the ribbon thickness, as shown in Figure 2. These are used here for the solution of the diffusion equation by the method of finite elements with boundary conditions representing ambient gas reactions with silicon melt.

The calculation domain encompasses the die top capillary and meniscus melt, with boundaries Γ_1 through Γ_6, the interface and the die inlet, as shown in Figure 2. Exact meniscus shapes can be calculated for the growth configurations modeled using the Laplace equation (8). Deviations of the exact contour from the straight lines used here for the meniscus (boundaries Γ_1 and Γ_2 in Figure 2) are not great enough to warrant a more precise representation given the accuracy of

the numerical transport equation solutions, which is typically about ten percent (7). The total meniscus surface area available for the reaction may be underestimated by five to ten percent with the contours Γ_1 and Γ_2. The impact of this approximation on the convective flow pattern is minimal because lateral flow velocities are small compared to the growth velocity.

The two-dimensional diffusion equation for impurity species of concentration C(x,y) and melt diffusion coefficient D is

$$D\left(\frac{\partial^2 C}{\partial x^2} + \frac{\partial^2 C}{\partial y^2}\right) = u\,\frac{\partial C}{\partial x} + v\,\frac{\partial C}{\partial y} \qquad (1)$$

u and v are the x- and y- components of the velocity field, respectively. With solute segregation at the interface, the boundary condition there is

$$-D\left(\frac{\partial C}{\partial x}\,n_x + \frac{\partial C}{\partial y}\,n_y\right) = \left(k_o\,\frac{\rho_\ell}{\rho_s} - 1\right) V_g n_y C \qquad (2)$$

n_x and n_y are the x- and y- components of the unit vector normal to the interface, and ρ_ℓ and ρ_s the liquid and solid silicon densities, respectively. V_g is the ribbon growth velocity and k_o the impurity segregation coefficient. The ribbon solute concentration C_S is calculated as $C_S = k_o C_I$, where C_I is the melt concentration evaluated at the interface. The melt inlet impurity concentration at the die top

base is $C = C_o$.

Meniscus surface and die inlet boundary conditions have been varied to model several cases of interest in ambient gas-meniscus melt reactions:

$$C_o = 0, \text{ die inlet, } C = 1 \text{ on } \Gamma_1 \text{ and } \Gamma_2 \qquad (3)$$

to represent meniscus source effects;

$$C_o = 1, \text{ die inlet, } C = 0,\ 0.5\ C_o,\ C_o \text{ on } \Gamma_1 \text{ and } \Gamma_2 \qquad (4)$$

to represent meniscus sink effects. Zero flux boundary conditions are maintained on die surfaces Γ_3, Γ_4, Γ_5, and Γ_6.

A choice must be made whether to apply the condition of Eq. (2) or a constant concentration, as expressed by Eqs. (3) or (4), at the meniscus surface-ribbon (interface) boundary when carrying out the numerical calculations. In the absence of experimental data to act as a guide, the results generated here have been obtained using Eq. (2). This yields variable ribbon surface concentrations, as illustrated by the results shown in Figure 3 to 5. In the other scheme, the use of a constant interface surface concentration equal to the meniscus source or strength value C_M fixes the ribbon surface concentration at $k_o C_M$. This results in higher average ribbon impurity concentrations in the case of meniscus sources, and lower averages for sinks, than obtained with the adopted scheme. However, the qualitative trends with meniscus height, ribbon thickness and growth speed exhibited by the data remain unaltered.

The die top geometry and growth parameters chosen are of interest in production of silicon ribbon for use as substrate material for solar cell fabrication (9): a die top height of L = 0.25 cm, capillary width W_1 = 0.025 cm and die top flat width W_2 = 0.005 cm; ribbon thicknesses from 0.01 to 0.03 cm and growth speeds from 0.02 to 0.06 cm/s were the other independent variables in the study. In the approach pursued in the modeling in Reference 7, temperature boundary conditions are treated as additional independent parameters and varied to generate solutions with different meniscus heights for a given ribbon thickness and growth velocity. The solutions employed here are those for which the meniscus height is consistent with solutions of the Laplace equation for a given set of growth parameters (7,8). Impurity parameters chosen for the calculations were $D = 5 \times 10^{-5}$ cm^2/s and k_o values of 1.25 and 0.07. The latter are representative of oxygen (10) and carbon (11), respectively. The value of D is that reported for carbon (12), while D is not known for oxygen. However, the value for carbon is in the lower range of those reported for impurities in silicon melt (6). This provides a lower bound estimate for meniscus source-induced melt impurity redistribution effects because they are essentially diffusion limited given a fixed growth speed.

Discussion

Normalized average impurity concentrations obtained from numerical solution of the transport equations are given in

Table I. Calculated impurity distributions through the ribbon thickness for a number of these cases are shown in Figures 3 to 5. Two aspects of the ambient gas-meniscus melt interaction have been modeled. Meniscus oxygen source effects are represented with the boundary condition of Eq. (3) and impurity parameters $k_o = 1.25$ and $D = 5 \times 10^{-5}$ cm^2/s; meniscus carbon sink effects are modeled with the conditions of Eq. (4) and $k_o = 0.07$ and $D = 5 \times 10^{-5}$ cm^2/s.

For a meniscus source, the average ribbon interface concentration increases with decreasing growth speed and increasing meniscus height (Table I and Figure 3). These trends are reversed with a sink operative (Table I and Figure 4). Growth speed has the most pronounced effect on ribbon impurity levels both for sources and sinks. This is shown in Figure 3, where the ratio of the ribbon center to the surface concentrations has changed dramatically by over two orders of magnitude, with an increase of V_g from 0.02 to 0.06 cm/s. Variations in the distribution with meniscus height and ribbon thickness are much less severe, as is evident from the data in Table I.

Figures 4 and 5 illustrate the dependence of the impurity distribution through the ribbon thickness on growth speed (Figure 4) and sink strength (Figure 3) for meniscus sinks. The distribution for case 4 in each of these figures is for a zero flux meniscus surface boundary condition. The solutions of the heat and momentum transport equations used for these

calculations result in interfaces which are concave toward the melt (7). This leads to $C_s/C_o > 1$ in the center of the ribbon cross section for an impurity with $k_o < 1$ because of lateral redistribution in the segregation boundary layer arising from interface curvature and melt convection. Even for a uniform meniscus source of strength equal to C_o, depletion of melt impurity levels is shown to occur (case 3, Figure 5). This takes place at the expense of the segregated impurity in the boundary layer, in which interface concentrations of the order of C_o/k_o drive the mass transfer across the meniscus surface.

The calculations show that oxygen transport from meniscus sources can account for the interstitial oxygen that is introduced in ribbon grown with a CO_2 ambient (1, 13). The highest ribbon concentration that has been observed is 10 ppma (14). This is about 15% of the maximum oxygen surface concentration of 69 ppma available with conditions of surface saturation. By comparison, calculated average ribbon oxygen concentrations are predicted to attain between 20% and 60% of a uniform meniscus source concentration (Table 1). Several factors associated with the experimental conditions and kinetic limitations for the transport processes modeled will lower the ribbon interstitial oxygen content below the maximum possible: (1) It is not known if the oxygen sources resulting from CO and CO_2 reactions with silicon melt can achieve melt surface saturation. The source strength there-

fore may never reach the 69 ppma shown to be possible with pure oxygen gas; (2) The EFG ribbon produced has a high defect density, and the interstitial oxygen need not represent the total oxygen content of the ribbon if oxygen is associated with these defects in non-interstitial sites; and (3) The presence of SiC on the meniscus surface may place a kinetic restriction on oxygen transport which is not present under conditions where pure oxygen is the ambient gas. Differences in the effects produced by CO and CO_2 have been observed. Die top deposits and meniscus surface film are heavier and interstitial oxygen levels lower with CO than with CO_2 for a given partial pressure. This can be explained if the former gas produces a higher percentage of SiC than other products and results in a reduced availability of oxygen to the melt interior (15).

The magnitude of the diffusion coefficient for oxygen in silicon melt is an adjustable parameter in the modeling. Calculations of impurity transport for EFG have shown that ribbon impurity redistribution is strongly dependent on the magnitude of D (6); the dependence on k_o when k_o is close to unity is very weak. These considerations apply also to the processes modeled here. Closer agreement between calculated oxygen levels and the measured average concentrations, that could be achieved by adjusting D, has not been sought because of the above uncertainties in experimental conditions.

The available experimental data do not shed light on am-

bient-related transport processes influencing ribbon carbon concentrations. Substitutional carbon measured by IR spectroscopy at the 16.5 μm band generally ranges from about 20 to 70 ppma (1 to 3.5 x 10^{18} at/cc) and does not show identifiable trends with gas species or partial pressures. From previous considerations of the Si-C phase diagram (1), it was estimated that ribbon total carbon levels are much higher, with the excess carbon incorporated into the ribbon as SiC by eutectic solidification. SiC is additionally observed to form on the die top surfaces (Γ_3 and Γ_4 in Figure 2), from which it is detached and incorporated into the ribbon as particles. This formation rate has been found to be influenced by ambient gas composition; since it would be expected to be dependent on the meniscus melt carbon level, this result supports the concept of meniscus sources and sinks for carbon. These competing processes for carbon transport in the die top melt must be better understood before specific effects due to meniscus surface reactions can be identified.

The calculated impurity concentrations in Table I and Figures 4 and 5 with C = 0 provide an upper bound (for the given D) for mass transport associated with processes involving impurity removal at the meniscus surface. The solutions of cases 2 and 3 in Figure 5 give the best representation of physical conditions involved in carbon depletion caused by SiC formation. The difference in carbon concentration between supersaturated interior melt and the melt in equili-

brium with the SiC particle at its surface gives the driving force for melt carbon depletion. For a particle temperature near the melting point of silicon, the latter concentration could be as high as 250 ppma but in all cases will be less than C_o. The meniscus melt carbon concentration is generally nonuniform and greater than C_o because of formation of the segregation boundary layer, which results in concentrations rising to as high as $C_o/k_o \sim 14\ C_o$ at the interface.

Removal of carbon and oxygen from the meniscus surface by evaporation of gases, such as CO and SiO, involves additional considerations. Evaporation is favored for meniscus ambient partial pressures below 3.8×10^{-4} atm for CO (5) and 8×10^{-3} atm for SiO (4) near the melting point of silicon. Diffusion through the surface gas boundary layer then limits mass transfer in the general case (16), while surface carbon and oxygen concentrations will not vanish. Impurity transport in this boundary layer falls outside of the scope of the present modeling. However, the solutions given in Figure 4 should be useful to represent evaporation processes in the limit of meniscus surface impurity concentrations C_M such that $C_M/C_o << 1$.

Summary

Numerical solutions of mass and momentum transport equations have been presented to model processes associated with ambient gas-meniscus melt reactions taking place during growth of silicon ribbon by EFG. Significant changes in

oxygen and carbon levels are predicted to be produced by meniscus surface sources and sinks, which are created through reaction of CO and CO_2 with silicon melt. The processes modeled can account for the level of interstitial oxygen, up to 10 ppma, that is observed to be introduced into ribbon grown with a CO_2 ambient from melt contained in graphite crucibles. Growth speed emerges as the process parameter with the most pronounced effect on ribbon impurity levels both for meniscus sources and sinks.

The study of carbon transport is complicated by the possibility that a second phase, SiC, forms in the interface region because of melt supersaturation by carbon. The SiC can act as a surface sink for carbon that significantly reduces levels of melt carbon.

ACKNOWLEDGEMENTS

We wish to thank Mr. F.V. Wald, Professor B. Chalmers, and Ms. M.C. Cretella for stimulating discussions during the preparation of this work, and Mr. G.M. Freedman for providing the IR spectroscopy data. This paper is based on work sponsored by the Jet Propulsion Laboratory, California Institute of Technology, under Subcontract No. 954355 under the Low-Cost Solar Array Project of DOE.

REFERENCES

1. J.P. Kalejs, M.C. Cretella, F.V. Wald and B. Chalmers, in: "Electronic and Optical Properties of Polycrystalline or Impure Semiconductors and Novel Silicon Growth Methods," K.V. Ravi and B. O'Mara, Eds., p. 242, The Electrochemical Society Softbound Symposium Series, Pennington, NJ (1980).
2. W. Kaiser and P.H. Keck, J. Appl. Phys. 28, 882 (1957); W. Kaiser and J. Breslin, J. Appl. Phys., 29, 1292 (1958).
3. J.A. Baker, in: "Semiconductor Silicon 1969," R.R. Haberecht and E.L. Kern, Editors, p. 566, The Electrochemical Society Softbound Symposium Series, Princeton, NJ (1969).
4. F. Schmid, C.P. Khattak, T.G. Diggs, Jr., and L. Kaufman, J. Electrochem. Soc., 126, 933 (1979).
5. Y. Endo, Y. Yatsurugi, Y. Terai and T. Nozaki, J. Electrochem. Soc., 126, 1422 (1979).
6. J.P. Kalejs, J. Cryst. Growth, 44, 329 (1978).
7. J.P. Kalejs, L.-Y. Chin and F. Carlson, paper presented at ACCG-5, San Diego, CA, July 1981; manuscript in preparation.
8. J.C. Swartz, T. Surek and B. Chalmers, J. Electron. Mater., 4, 255 (1975).
9. J.P. Kalejs, B.H. Mackintosh, E.M. Sachs and F.V. Wald,

14th IEEE Photovoltaic Specialists Conference Record (New York: IEEE; 1980), p. 13.

10. The value of k_o for oxygen is not known accurately, but is believed to be of the order of unity. $k_o = 1.25$ is taken as representative for the present calculation; see also T. Nozaki, Y. Yatsurugi, N. Akiyama, Y. Endo and Y. Makide, J. Radioanal. Chem., 19, 109 (1974); Y. Yatsurugi, N. Akiyama, Y. Endo and T. Nozaki, J. Electrochem. Soc., 120, 975 (1973).
11. T. Nozaki, Y. Yatsurugi and N. Akiyama, J. Electrochem. Soc., 117, 1566 (1970).
12. G.G. Gnesin and A.I. Raichenko, Poroshkovaya Met., 13, 35 (1973).
13. J.P. Kalejs et al., DOE/JPL 954355, Quarterly Progress Report, May 1981.
14. The ribbon interstitial oxygen concentration is obtained by low temperature (80°K) infrared spectroscopy at the 9 μm band and ASTM Procedure F-121.
15. F.V. Wald et al., DOE/JPL 954355, Quarterly Progress Report, October 1980.
16. C. Wagner, J. Appl. Phys. 29, 1295 (1958).

TABLE I

Calculated Average Impurity Concentrations ($\overline{C}$) in a Plane Through the Ribbon Cross Section Normal to the Growth Direction as a Function of Growth Conditions and Impurity Species Parameters with Meniscus Sources and Sinks. All Results are for $D = 5 \times 10^{-5}$ cm^2/s.

Growth Parameters			Normalized Impurity Concentration	
Speed (cm/second)	Thickness (cm)	Meniscus Height (cm)	$k_o = 1.25$; Meniscus Sources $(\overline{C}/C_M)^\dagger$	$k_o = 0.07$; Meniscus Sinks $(\overline{C}/C_o)^*$
0.02	0.02	0.018	0.40	0.39
0.03	0.02	0.021	0.32	0.65
0.04	0.02	0.020	0.24	0.78
0.02	0.02	0.026	0.50	0.33
0.02	0.03	0.026	0.35	0.44
0.04	0.01	0.027	0.56	0.88
0.04	0.02	0.027	0.32	0.77
0.06	0.02	0.026	0.17	0.80

$^\dagger C_M$ is the imposed uniform meniscus surface concentration.

$^* C_o$ is the uniform die top inlet melt concentration.

FIGURE CAPTIONS

Figure 1 Schematic of crucible and die configuration used in cartridge mode of preparation of silicon ribbon by EFG.

Figure 2 Cross section taken through die top and meniscus in ribbon thickness plane showing location and boundaries of calculation domain.

Figure 3 Calculated impurity distributions through ribbon thickness for uniform meniscus source concentration $C = C_M$ and impurity parameters $k_o = 1.25$ and $D = 5 \times 10^{-5}$ cm^2/s. Results are for a constant ribbon thickness of 0.02 cm and meniscus height of 0.026 cm, and growth speeds of 0.02 cm/s (case 1), 0.04 cm/s (case 2), and 0.06 cm/s (case 3).

Figure 4 Calculated impurity distributions through ribbon thickness for uniform meniscus sink concentration $C = 0$ and impurity parameters $k_o = 0.07$ and $D = 5 \times 10^{-5}$ cm^2/s. Results are for constant ribbon thickness of 0.02 cm and meniscus height of 0.020 cm, and growth speeds of 0.02 cm/s (case 1), 0.03 cm/s (case 2) and 0.04 cm/s (case 3). Case 4 is a reference distribution for 0.02 cm/s for zero flux ($\partial C/\partial n = 0$) meniscus surface boundary conditions.

Figure 5 Calculated impurity distribution through ribbon thickness as a function of meniscus sink strength: (1) $C = 0$; (2) $C = 0.5\ C_o$; (3) $C = C_o$; and (4) $\partial C/\partial n = 0$. Constant ribbon thickness of 0.020 cm, meniscus height 0.026 cm and growth speed 0.02 cm/s; impurity parameters are $k_o = 0.07$ and $D = 5 \times 10^{-5}$ cm/s.

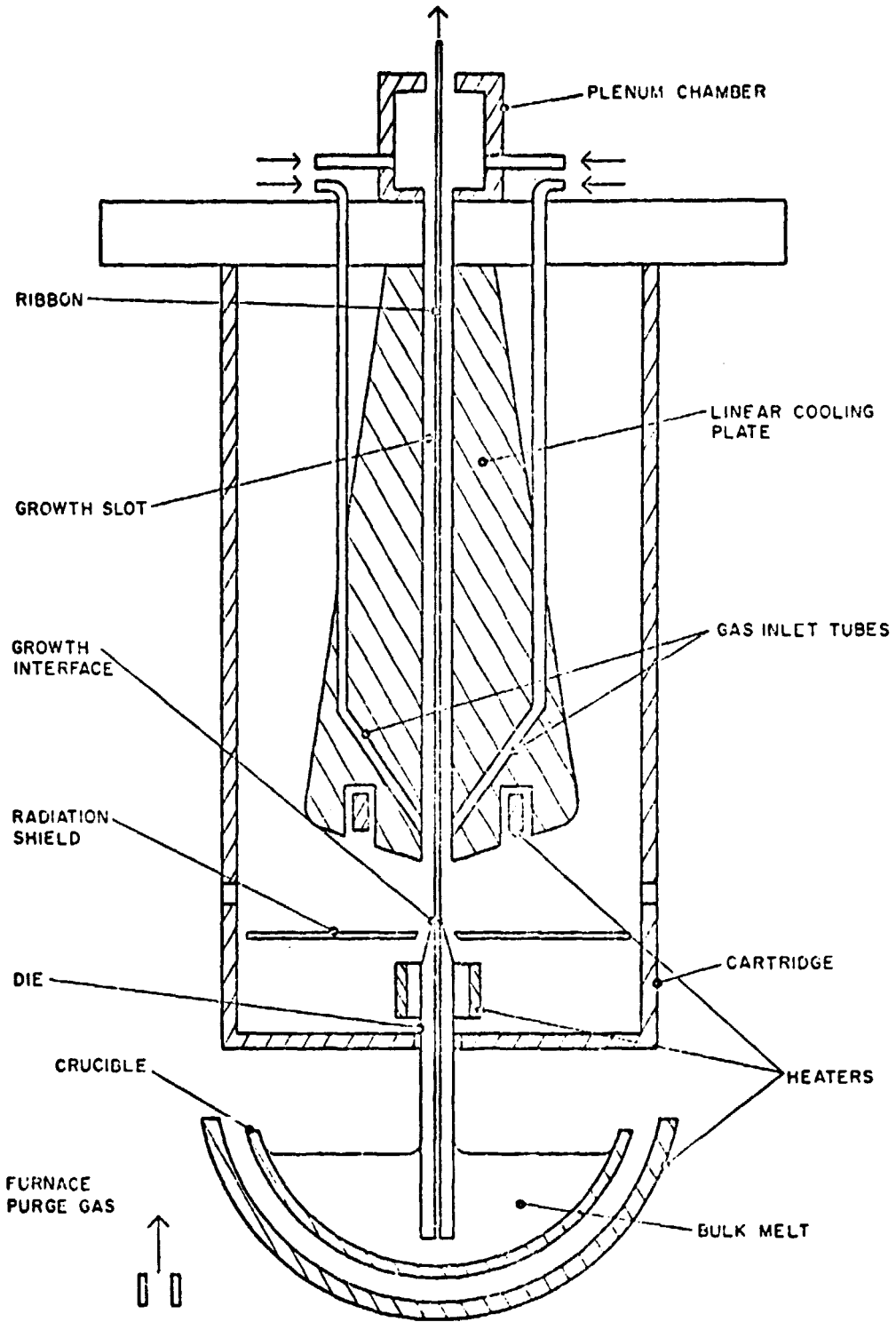

Figure 1

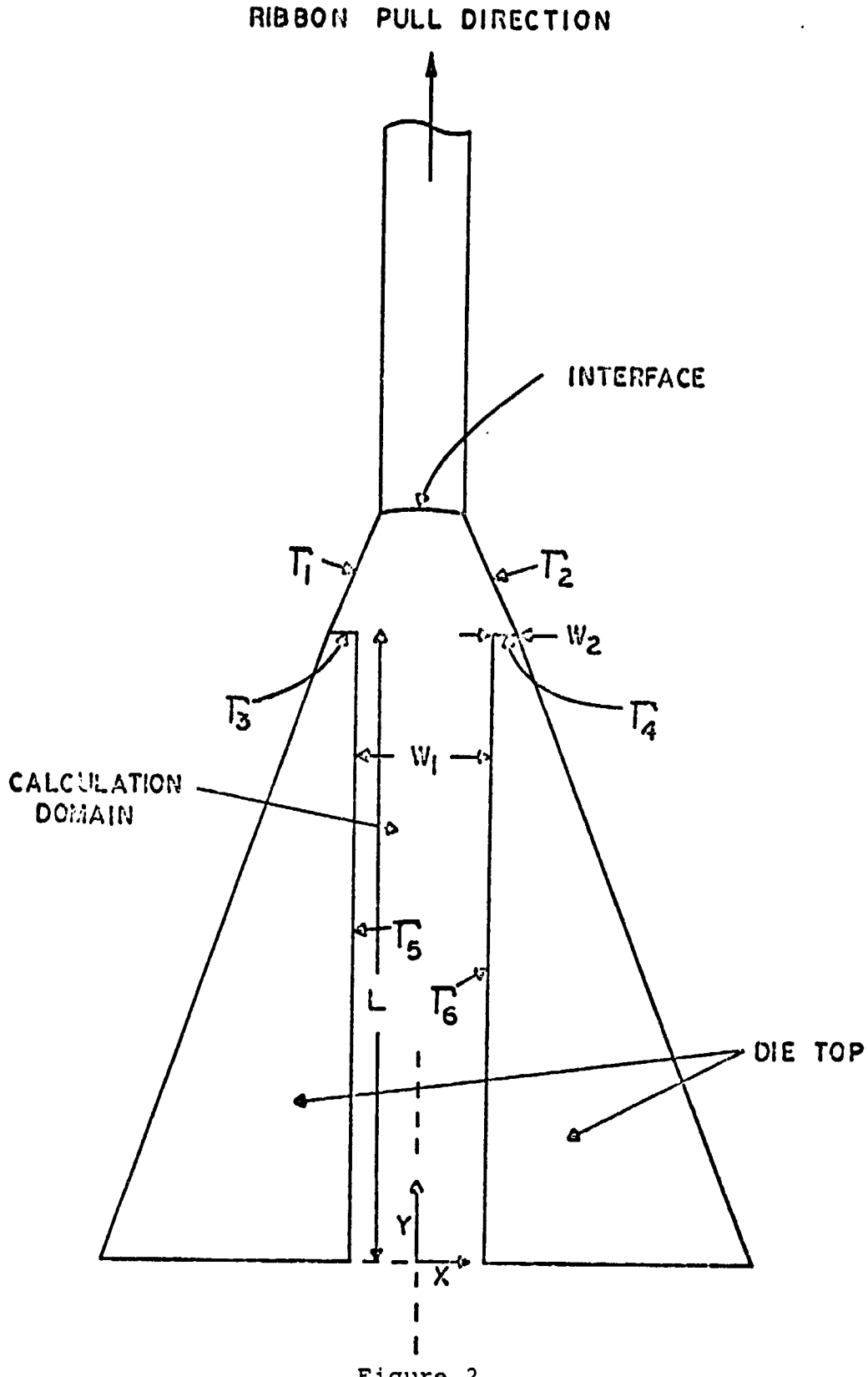

Figure 2

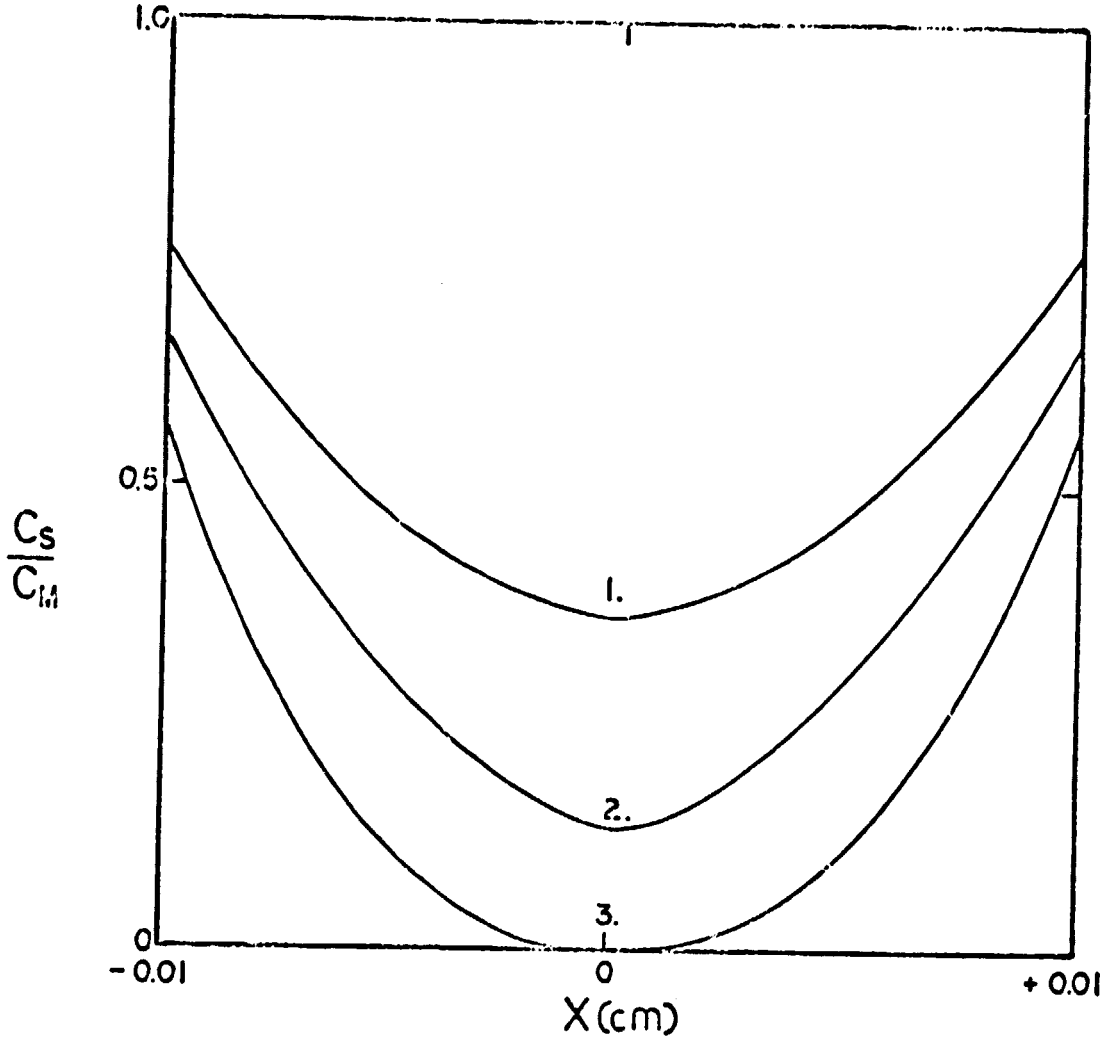

Figure 3

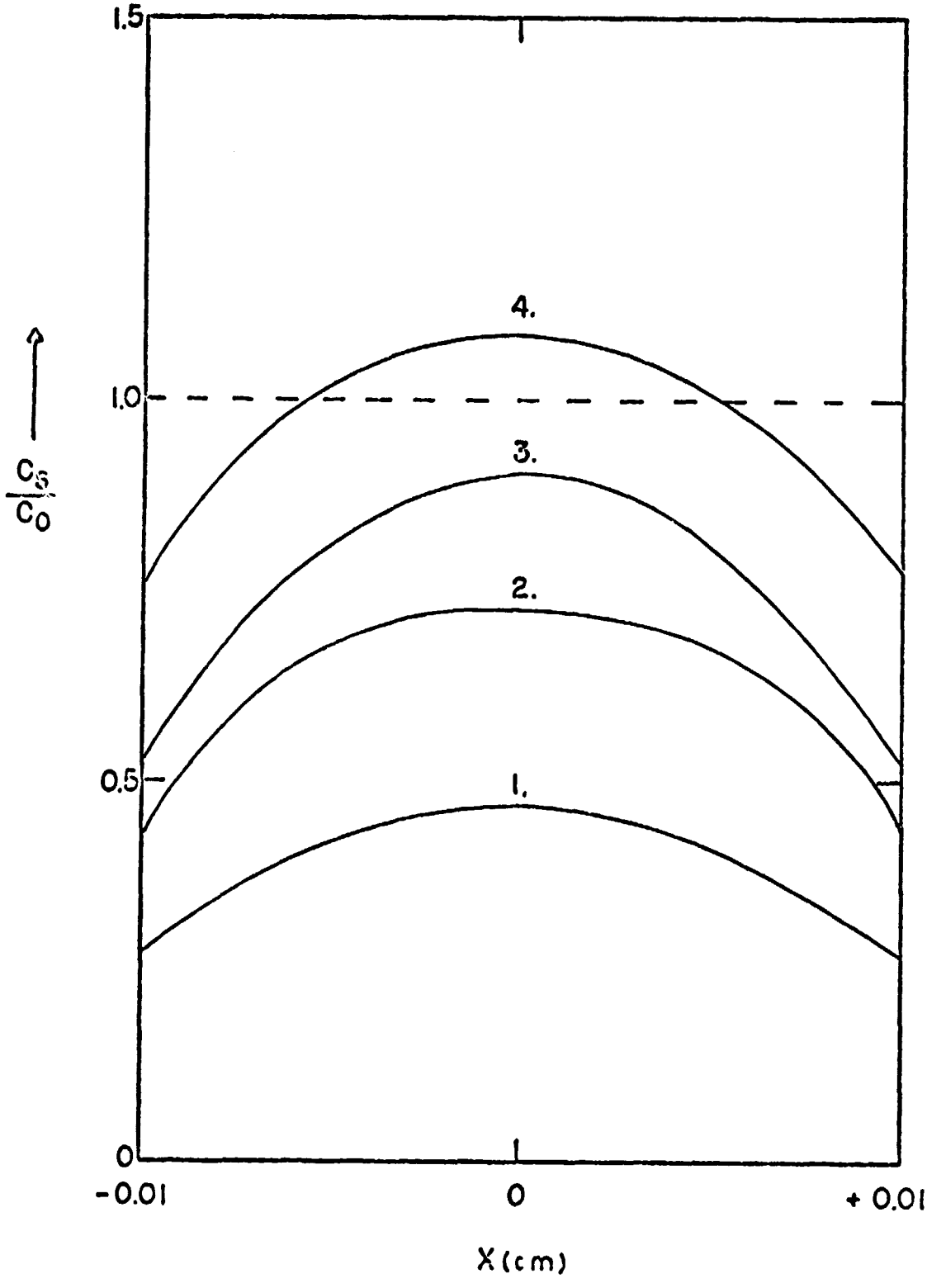

Figure 4

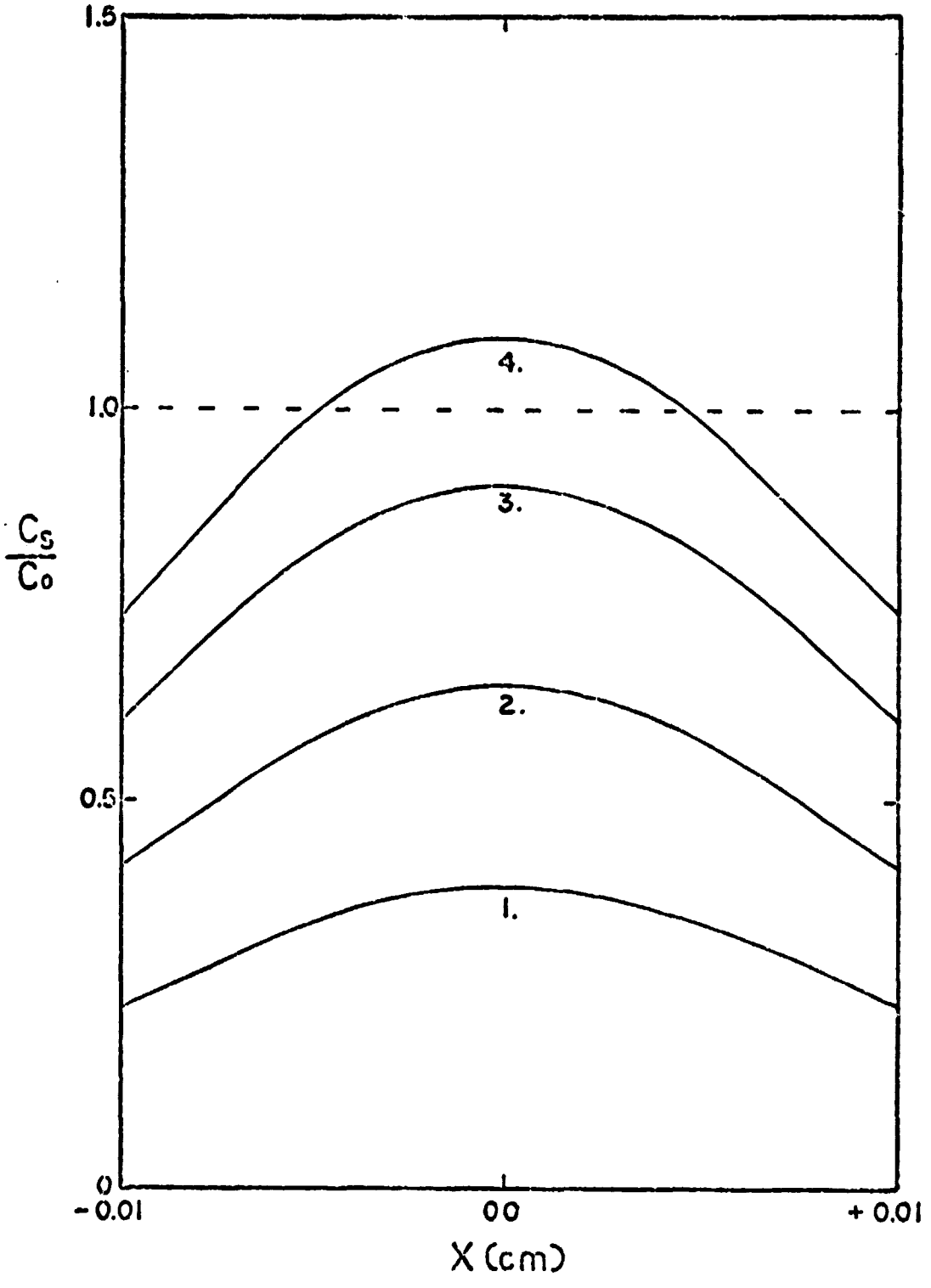

Figure 5

APPENDIX 8(b)

phys. stat. sol. (a) 67, 103 (1981)

Subject classification: 13.4; 14.3; 22.1.2

Mobil Tyco Solar Energy Corporation, Waltham[1])

Some Aspects of the Effect of Heat Treatment on the Minority Carrier Diffusion Length in Low Resistivity p-Type Silicon

By

C. T. Ho and F. V. Wald

Four different types of low resistivity p-type silicon, namely float-zoned and Czochralski-grown materials as well as EFG-grown ribbons containing high and low oxygen concentrations are subjected to heat treatments between 850 and 1050 °C, followed by slow cooling to 600 °C, after which they are air quenched. Subsequently, the response of their electron diffusion lengths to the flux of 1 μm photons is measured. The results show that in all materials a progressive destruction of the minority carrier diffusion length occurs as the heat treatment temperature increases. However, it appears that the dominant recombination centers in the oxygen rich materials differ from those present in the relatively oxygen free materials. It is concluded that a "gettering" effect based on oxygen occurs, which is not likely to be related to SiO_2 precipitation, however.

Es wird das Verhalten der Elektronendiffusionslänge in Bor-dotiertem Silizium als Funktion des Photonenflusses bei 1 μm Wellenlänge in Abhängigkeit von vorhergegangenen Wärmebehandlungen des Materials untersucht. Dazu werden vier Arten von Silizium, nämlich tiegelfrei gezogenes (FZ), tiegelgezogenes (CZ) und sauerstoffarme (OL) sowohl als auch sauerstoffreiche (OR) Bänder die im EFG-Verfahren hergestellt waren, bei Temperaturen zwischen 850 und 1050 °C vorgetempert und anschließend langsam auf 600 °C abgekühlt; danach werden sie an Luft abgeschreckt. Die Untersuchungen ergeben, daß bei allen Materialien eine Reduktion der Elektronendiffussionslänge eintritt, wenn bei höheren Temperaturen vorbehandelt wird. Allerdings scheinen sich die erzeugten Rekombinationszentren in den sauerstoffreichen Materialien von denen in den sauerstoffarmen zu unterscheiden. Es wird geschlossen, daß sich größere Komplexe zwischen Sauerstoff-Silizium und Verunreinigungen bilden, bevor es zur Präzipitation von SiO_2 kommt.

1. Introduction

Recently we have shown that the introduction of oxygen into EFG ribbon during growth can have profound consequences in altering the morphology of the resulting material and in improving its electronic properties [1]. We could also show that these improvements may be translated into clearly more efficient solar cells and that oxygen may be introduced both by use of quartz crucibles and by the introduction of suitable oxygen-bearing gases around the liquid meniscus during growth [2].

It has also become quite clear that it is the presence of oxygen in the ribbon that causes the previously observed "light enhancement effect" which manifests itself by an increase of the minority carrier diffusion length with the increasing photon flux. This may be interpreted as resulting from the filling of a number of closely spaced donor-like recombination states in the lower half of the gap as the electron Fermi level moves further upward with the increasing non-equilibrium electron population

[1]) 16 Hickory Drive, Waltham, Massachusetts 02254, USA.

injected into the material by the photogeneration process [3]. In a subsequent investigation, Pogany confirmed this interpretation, and also experimentally showed that such effects cannot be produced by one or a few simple impurity levels [4].

Thus, to us, the close spacing of these levels and their nearly Gaussian distribution through the gap has always suggested rather more complex structures for the centers which cause these effects and since they appear to be largely absent in oxygen-free material [2], oxygen must be implicated in their formation.

2. Experiments and Results

In this paper then, we present the results of a quantitative comparison of the changes in minority carrier diffusion length as a function of the flux of photons of wavelength 1 μm [5]. The characteristics of four different types of silicon materials, heat-treated through three differing sequences were compared. The materials were:

(i) Single-crystal float-zoned samples, boron doped to ≈ 1 Ω cm with a starting average electron diffusion length of ≈ 160 μm as measured by a surface photovoltage method [6].

This material also was analyzed for carbon and oxygen using standard infrared transmission techniques [7] and both of these elements were found to lie below a concentration of ≈ 1×10^{16} and 2×10^{16} atoms cm^{-3}, respectively. These are the detection limits for our case, as we used relatively thin slices for the studies here.

(ii) Single-crystal Czochralski-grown slices, boron doped to ≈ 2 Ω cm with a starting diffusion length of ≈ 135 μm, a carbon content of 3×10^{17} atoms cm^{-3} and also containing 2×10^{18} atoms cm^{-3} of oxygen.

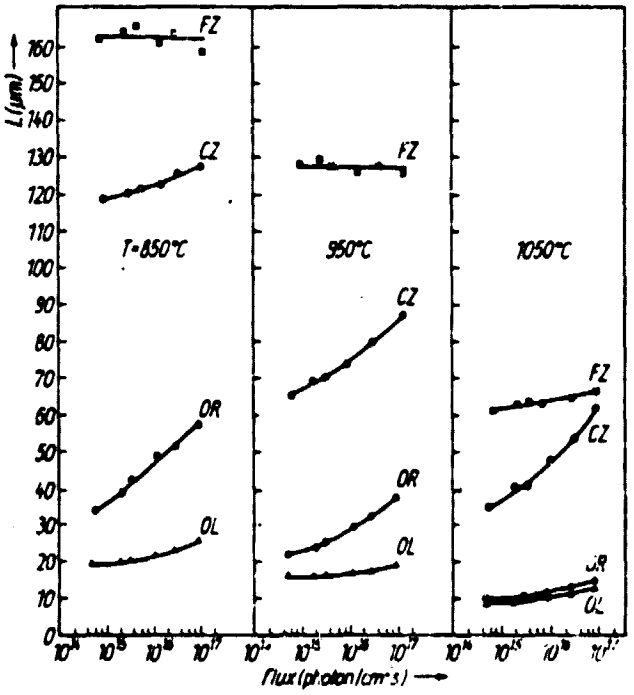

Fig. 1. The effect of pre-annealing temperature (see text) on the response of the electron diffusion length L to the flux of 1 μm photons, for various kinds of p-type silicon

(iii) 5 cm wide EFG ribbons, nominally 1 Ω cm boron doped, grown at ≈ 2 cm/min from a graphite crucible and using a graphite die. Oxygen was introduced into these ribbons by controlling the CO_2 concentration around the meniscus [1]. When no CO_2 was introduced into the gas ambient (the CO_2-off condition [2]), the oxygen concentration in this ribbon was found to be $\leq 2 \times 10^{16}$ atoms cm^{-3}, i.e. below our detection limit, whereas carbon was found at $\approx 1 \times 10^{16}$ atoms cm^{-3}. For this material, which we designate "oxygen lean" (OL), the electron diffusion length averaged ≈ 34 μm.

(iv) Material from the same growth run, when CO_2 was added to the argon ambient around the meniscus, increased in diffusion length to ≈ 48 μm. This "oxygen rich" (OR) material now contained 4×10^{17} atoms cm^{-3} of oxygen and $\approx 1 \times 10^{16}$ atoms cm^{-3} of carbon. Of course, all ribbons contained the usual sets of defects inherent in EFG-grown silicon [8 to 10].

These four types of material, namely FZ (float zoned), CZ (Czochralski grown), OL (EFG ribbon grown under ambient conditions relatively free of oxygen), and OR (ribbon where CO_2 was introduced during growth), were all subjected to three annealing cycles in a phosphine containing atmosphere and at temperatures of 850, 950, and 1050 °C, using a standard diffusion tube furnace. The atmospheric and temperature conditions thus are similar to various diffusion sequences which one might use in solar cell preparation. However, in order to drive any solid-state reactions further to completion, the time at these three temperatures was extended to 90 min and in each case a slow cooling sequence was subsequently used which brought the slices down to 600 °C over 5 h, after which they were removed from the diffusion tube and air quenched.

The results of these experiments are all summarized in Fig. 1.

3. Discussion and Conclusions

It is quite clear from Fig. 1 that the heat treatment sequences employed here did have a significant effect on the final minority carrier lifetime of all the materials investigated, whether they contained high oxygen concentrations or not. We observe quite generally a progressive destruction of diffusion length as the pre-annealing temperature increases, irrespective of the fact that the subsequent slow cooling sequence exposes all materials for a significant length of time to temperatures around 600 to 800 °C.

This effect seems also not easily explained by assuming that impurity in-diffusion occurs from the annealing furnace or the atmosphere during the heat treatments. Since both the FZ and CZ materials were heat treated in the same furnace, they should have been exposed to the same impurity concentrations and should then be expected to show very similar diffusion lengths for the two higher temperature pre-anneals. That is however not the case, and one is therefore forced to assume that the observed decreases in diffusion length are due to internal rearrangements of recombination centers, i.e. centers which were not "active" for recombination in the as-grown material are now "active" after the heat treatment.

Such effects have been previously shown by Graff and Pieper [11] to exist in float-zoned material. They demonstrated that the lifetime of such crystals could be either increased or decreased in the temperature range between 600 and 900 °C, depending on the general defect concentration (dislocations, swirls, "A" and "B" clusters), and they associated the lifetime increases with an "internal gettering effect", caused by unspecified point defect complexes. It would then be possible to interpret the results of our experiments in this view, by saying that certain point defect complexes which may also incorporate bound impurities are progressively destroyed as the initial

annealing temperature is increased, even though the cooling schedule is held relatively constant.

That effect clearly manifests itself (Fig. 1) in the float-zoned material and is quite total for the EFG material with its far higher defect and impurity contents. In fact, we have observed on occasion even more pronounced cases than those indicated in Fig. 1, where EFG material with an initial diffusion length of 70 to 100 μm was obtained in growth from graphite crucibles under oxygen-lean conditions, which was then reduced to a level of 20 to 25 μm during subsequent solar cell fabrication.

In other words, for all materials, whether they contain oxygen or not, in which pre-annealing and the slow cool are combined, a progressive destruction of the diffusion length with increased pre-annealing temperature is observed. Hence, it appears that during crystal growth of silicon at high temperatures a general "gettering" effect prevails, which is perhaps based on the "metal point defect" association model suggested by Graff and Pieper [11]. This association, however, appears to be quite unstable at lower temperatures and thus in all materials a reduction in lifetime occurs when they are heated for any duration in the temperature range between 1050 and 800 °C.

However, when oxygen is present in larger concentrations, this effect can apparently be counteracted somewhat, at least for heat treatments at intermediate temperatures. We conclude this of course from the fact that the diffusion length is now very sensitive to the photon flux, which indicates the presence of a set of quite different recombination centers in the oxygen-rich materials, which now clearly dominate the lifetime and which must have therefore been formed by an attraction between oxygen and those centers which dominate the lifetime in the oxygen-lean materials.

The cooling schedule used here indicates that the crystals are annealed for a considerable length of time at temperatures around 700 °C, but are quite quickly cooled through all temperatures below 600 °C so that we may assume that the present results are not due to effects associated with the well-known "thermal donor", whose effect is maximized at 450 °C. In fact, most investigations suggest that this "thermal donor" is destroyed at temperatures over 600 °C [12]. However other, more complex, donors [13] which are believed to take the form of larger Si_xO_y clusters and whose occurrence is maximized around 700 °C have recently been discussed [12, 14]. Thus we postulate that in our oxygen containing material these larger clusters play a role in the gettering of impurities. Such clusters of course can be viewed as part of a continuum which eventually leads to SiO_2 precipitation [15] and the sensitivity of such precipitation reactions to carbon content and pre-annealing temperature of silicon crystals has been well established recently [16, 17].

However, we do not believe that in this case the impurity gettering capability of the clusters is related to their eventual precipitation as SiO_2, which then generates dislocations that act as impurity sinks [18] since for "EFG"-grown ribbon with its relatively high defect contents [8 to 10] such an explanation seems hardly tenable. Yet our diffusion length measurements suggest that gettering by oxygen does in fact occur, and indeed is sensitive to the pre-annealing treatments which the material undergoes. It is then our postulate that larger Si_xO_y aggregates "getter" metallic impurities prior to the precipitation stage, by mechanisms not related to dislocations, but perhaps through coulombic attraction or physico-chemical forces of other kinds. However, it is quite possible that dislocations play a role in the initial nucleation of such aggregates.

Acknowledgements

The authors are grateful for the excellent work of Mr. J. Mathias on the diffusion length measurements, and the determinations of oxygen and carbon content which

have been carried out by Ms. M. Cretella and Mr. G. Freedman, as well as for many valuable discussions with Dr. J. P. Kalejs. Also, part of the work was carried out as a special task of a project on EFG sheet growth under Jet Propulsion Laboratory contract No. 954355, Large Scale Solar Array (LSA) project, U.S. Department of Energy.

References

[1] J. P. Kalejs, M. C. Cretella, F. V. Wald, and B. Chalmers, ECS Meeting, St. Louis, May 1980 (Abstract No. 329); Proc. Symp. Electronic and Optical Properties of Polycrystalline or Impure Semiconductors and Novel Silicon Growth Methods, Ed. K. V. Ravi and O'Mara, The Electrochemical Society, Princeton 1980 (p. 242).
[2] B. Mackintosh, J. P. Kalejs, C. T. Ho, and F. V. Wald, III. E. C. Photovoltaic Solar Energy Conference, Ed. W. Palz, D. Reidel, Dordrecht 1981 (p. 553).
[3] C. T. Ho, R. O. Bell, and F. V. Wald, Appl. Phys. Letters 31, 463 (1977).
[4] A. Pogany, XIV. IEEE Photovoltaic Specialists Conf. Record, IEEE, New York 1980 (p. 140).
[5] J. Ho and J. Mathias, IEEE Trans. Electron Devices 25, 1332 (1978).
[6] R. O. Bell and G. M. Freedman, XIII. IEEE Photovoltaic Specialists Conf. Record, IEEE, New York 1978 (p. 89).
[7] ASTM Standard, F 121-79, and ASTM Standard, F 123-74, American Society for Testing and Materials, Philadelphia (PA) 1980.
[8] K. V. Ravi, J. Crystal Growth 39, 1 (1977).
[9] K. Yang, G. H. Schwuttke, and T. F. Ciszek, J. Crystal Growth 50, 301 (1980).
[10] C. V. H. N. Rao, M. C. Cretella, F. V. Wald, and K. V. Ravi, J. Crystal Growth 50, 311 (1980).
[11] K. Graff and H. Pieper, J. electronic Mater. 4, 281 (1975).
[12] V. Cazcarra and P. Zunino, J. appl. Phys. 51, 4206 (1960).
[13] A. Kanamori and M. Kanamori, J. appl. Phys. 50, 8095 (1980).
[14] D. Wruck and P. Gaworzewski, phys. stat. sol. (a) 56, 557 (1979).
[15] M. Tajima, S. Kishino, M. Kanamori, and T. Lisaka, J. appl. Phys. 51, 2247 (1980).
[16] S. Kishino, Y. Matsushita, and M. Kanamori, Appl. Phys. Letters 35, 213 (1979).
[17] K. Yamamoto, S. Kishino, Y. Matsushita, and T. Lisuka, Appl. Phys. Letters 36, 195 (1980).
[18] T. Y. Tan, E. E. Gardner, and W. K. Tice, Appl. Phys. Letters 30, 175 (1977).

(Received June 4, 1981)